

Generalized Sidelobe Canceller for Time-Domain Region-of-Interest Beamforming

Joel S. , *Student Member, IEEE*, Ariel Frank , Israel Cohen , *Fellow, IEEE*,
and Nithin V. George , *Member, IEEE*

Abstract—One of the key challenges in array signal processing is the lack of precise source location information, which can arise from estimation errors or the presence of a moving source. Conventional beamformers, which rely on accurate spatial information, perform suboptimally under such conditions. Region-of-interest (ROI) beamformers address this limitation by focusing on a spatial region rather than a single direction. In this work, we introduce a new ROI beamformer based on the generalized sidelobe canceller (GSC) framework with time-domain convolutive filters. The proposed beamformer can concentrate on a specified ROI while suppressing noise and interference from other directions. To evaluate the efficacy of the proposed beamformer, we derive several performance metrics. Then we analyze various blocking matrix designs, focusing on signal leakage as a key factor in interference suppression without distorting the desired signal. Furthermore, an adaptive implementation based on the recursive least-squares (RLS) algorithm is developed, along with a low-complexity variant using the nearest Kronecker product (NKP) approximation. Simulation results demonstrate the effectiveness of the proposed ROI-GSC beamformer.

Index Terms—Blocking matrix, broadband beamforming, generalized sidelobe canceller (GSC), microphone array, nearest Kronecker product, region-of-interest beamforming.

I. INTRODUCTION

MICROPHONE arrays leverage optimal beamforming techniques for various tasks, including speech enhancement and noise reduction [1], [2], source detection and localization [3], and speech recognition [4], [5]. These techniques enhance signals of interest while suppressing unwanted noise by exploiting spatial information captured by the array [6], [7]. Over decades of research, beamforming has evolved into

a foundational component in radar, wireless communications, and acoustic signal processing [8], [9], [10]. More recently, beamforming using microphone arrays has gained prominence in applications such as smart home devices and conference room setups, enabling remote participation and enhanced user experiences [11].

One widely known beamformer is the generalized sidelobe canceller (GSC). The GSC beamformer is designed under the assumption that the source's direction of arrival (DOA) is known in advance [12]. While numerous studies have examined the GSC framework [13], [14], [15], [16], [17], practical scenarios often lack accurate directional information due to limited prior knowledge of the DOA, source movement, and estimation errors.

To address the challenges posed by uncertain DOA information or look-direction error, a wide range of robust beamforming techniques have been developed, which can be broadly grouped into frequency domain [18], [19], [20], [21], [22], [23], [24], [25], [26], [27], [28], [29], [30], [31], time-frequency domain [32], [33], [34] and, time domain [35], [36], [37], [38] methods. In the first category, Doles and Benedict [18] introduced a frequency-domain approach to design a beamformer with a frequency-invariant beampattern. Further approaches include leveraging the two-dimensional Fourier transform property for equally spaced arrays [19] and utilizing a beam-space implementation [20]. A polynomial beamforming method based on a least-squares beampattern approximation technique was developed by Mabande and Kellermann [21]. Zhu and Wu [22] proposed a frequency-invariant beamformer developed through an adaptive synthesis method for wideband array design. By keeping the beampattern constant with frequency, frequency-invariant designs prevent signal distortion under DOA mismatch; however, attenuation increases with angular offset from the mainlobe center, thereby reducing array gain. An approach that synthesizes a constant beamwidth multi-beam by superimposing multiple marginally steered single beams is discussed in [25]. Various other constant beamwidth beamformer designs utilizing uniform linear arrays and uniform concentric circular arrays are discussed in [23], [24], [26], [27], [28], and the modeling of scattered sources is further explored in [29], [30]. The second category involves time-frequency approaches. In this category, Davis et al. [32] introduced a time-frequency domain subband adaptive beamforming framework, considering a space-constrained source model. Furthermore, in [33], an acoustic spotformer was developed to capture the signals from the spot of interest while effectively suppressing noise and

Received 11 May 2025; revised 28 September 2025 and 15 December 2025; accepted 16 January 2026. Date of publication 23 January 2026; date of current version 2 February 2026. This work was supported in part by the Department of Science and Technology, Government of India under the MATRICS Scheme MTR/2022/000290, in part by Overseas Research Experience Fellowship, TEOCO Chair of the Indian Institute of Technology Gandhinagar, the Israel Science Foundation under Grant 1449/23, and in part by the Pazy Research Foundation. The associate editor coordinating the review of this article and approving it for publication was Dr. Ina Kodrasi. (*Corresponding author: Joel S.*)

Joel S. and Nithin V. George are with the Department of Electrical Engineering, Indian Institute of Technology Gandhinagar, Gujarat 382055, India (e-mail: joel.s@iitgn.ac.in; nithin@iitgn.ac.in).

Ariel Frank and Israel Cohen are with the Andrew and Erna Viterbi Faculty of Electrical and Computer Engineering, Technion – Israel Institute of Technology, Haifa 3200003, Israel (e-mail: arielfrank@campus.technion.ac.il; icohen@ee.technion.ac.il).

Digital Object Identifier 10.1109/TASLPRO.2026.3657239

interference. The study in [34] developed a spatially robust GSC beamformer with controlled white noise gain (WNG) and examined the relationship between the WNG and spatial robustness. The third category involves time domain approaches. Within the time-domain class, a beamformer employing an adaptive array system with direction constraints is studied in [35], which also explores the impact of errors in setting the constraints. Further, a robust beamformer that uses an adaptive blocking matrix and a norm-constrained noise canceller that addresses steering vector errors is discussed in [37]. Additionally, a beamforming method with regional constraints for designing robust adaptive beamformers in the near field is studied in [38] and provides robustness to location errors by utilizing constraints of unity gain across the desired region. Frank and Cohen [39] proposed a time-domain ROI beamformer as a practical approach to handling unknown-DOA scenarios. Their proposed least-distortion maximum gain (LDMG) beamformer selectively emphasizes signals originating from a desired region while reducing the impact of noise and interference from other directions.

In contrast to earlier time-domain approaches that depended on the assumed simplified near-field [38] or far-field propagation models [35], [37], [40], [41] in anechoic conditions or depend on acoustic transfer functions [36], our framework is built on relative impulse responses that provide a more accurate representation of reverberant environments. Relative impulse responses capture the acoustic differences between microphones relative to a chosen reference sensor, and they are typically much shorter in duration than full transfer functions. This reduces filter length requirements, which in turn lowers computational load. Since fewer coefficients must be estimated, parameter estimation is simplified, leading to improved robustness. Building on this motivation, this work proposes an optimal time-domain GSC beamformer specifically designed for ROI applications. To begin, we define key performance metrics for ROI beamformers and implement the proposed approach by diagonalizing the desired ROI matrix, allowing thereby obtaining a-independent and data-dependent beamformer weights. Additionally, an investigation is conducted into the development of blocking matrices for an ROI. We focus on its impact on signal leakage, a critical factor that affects the beamformer's ability to suppress interference while preserving the desired signal. The effectiveness of the proposed beamformer is thoroughly evaluated through a series of simulations. Furthermore, we developed an adaptive implementation of the proposed ROI-GSC beamformer using the least mean squares (LMS) and recursive least-squares (RLS) algorithms, and we also derived the optimal Wiener solution for the ROI LMS-GSC beamformer. Furthermore, we employed the nearest Kronecker product (NKP) approach to the ROI RLS-GSC beamformer weights to reduce computational cost. By controlling the rank of the proposed structure, the NKP approach enables a tradeoff between computational complexity and beamforming performance. The Kronecker decomposition framework has been applied in various domains, demonstrating its effectiveness [42], [43], [44], [45], [46], [47], [48], [49], [50], [51]. The NKP approach presented in this work is a generalization of prior Kronecker product beamformers [52], [53] by extending the focus from a single look-direction to a

ROI subspace constraint. This NKP based ROI definition uses relative impulse responses to accurately capture reverberation, avoiding the simplified far-field model in anechoic assumptions mentioned in previous Kronecker product studies [52], [53].

The structure of this paper is as follows: Section II outlines the signal model and problem formulation. Section III defines the proposed methodology. Section IV defines performance measures to analyze the proposed ROI-GSC beamformer. Section V discusses the simulation results obtained in a reverberant environment and compares the performance of the proposed beamformer with that of state-of-the-art methods. Finally, Section VI summarizes the conclusions.

Notations: $(\cdot)^T$ refers to the transpose operator, $*$ denotes linear convolution, $\mathbb{E}(\cdot)$ is the expectation operator, and $\text{tr}(\cdot)$ is the trace operator.

II. SIGNAL MODEL AND PROBLEM FORMULATION

Let $s(k)$ represent a desired source signal originating from a far-field source located in the angular direction (θ_q, ϕ_q) , where θ_q is the polar angle and ϕ_q is the azimuthal angle in a spherical coordinate system. An array of N sensors is used to capture a convolved version of the desired signal in a noisy environment. At a given discrete time instant k , the received signals can be represented as

$$\begin{aligned} u_n(k) &= h_n(k) * s(k) + v_n(k) \\ &= s_n(k) + v_n(k), \quad n = 1, 2, \dots, N, \end{aligned} \quad (1)$$

where $h_n(k)$ denotes the impulse response from the source location to the n th sensor and $v_n(k)$ is the additive noise in the n th sensor. The signals $s_n(k)$ and $v_n(k)$ are assumed to be statistically independent, real, stationary, and broadband. The signals $s_n(k)$, $n = 1, 2, \dots, N$, have coherence with each other, whereas $v_n(k)$, $n = 1, 2, \dots, N$, have partial coherence. Most of the expressions in this paper are functionally dependent on the angular direction of the source, e.g., $h_n(k)$ and $s_n(k)$. However, for ease of reading, the dependency on (θ_q, ϕ_q) is omitted. Considering Sensor 1 as the reference sensor, (1) can be rewritten as follows:

$$u_n(k) = r_n(k) * s_1(k) + v_n(k), \quad n = 1, 2, \dots, N, \quad (2)$$

where $r_n(k)$ represents the relative impulse response from the source location to the n th sensor, relative to Sensor 1, which satisfies the following two equations:

$$r_1(k) = \delta(k), \quad (3)$$

$$r_n(k) * s_1(k) = h_n(k) * s(k), \quad n = 2, \dots, N, \quad (4)$$

where $\delta(k)$ is the Kronecker delta. The relative impulse responses are approximated as non-causal filters with a finite length of L_q so that (2) can be approximated as

$$u_n(k) = \sum_{t=-\Delta}^{L_q-1-\Delta} r_n(t) s_1(k-t) + v_n(k), \quad n = 1, 2, \dots, N. \quad (5)$$

Here, Δ represents the number of non-causal time samples used for approximating (2). The values of $r_n(t)$ outside the set $t \in \{-\Delta, \dots, L_q - 1 - \Delta\}$ are assumed to be negligible.

We can represent (5) in a vectorized form as

$$u_n(k) = \mathbf{r}_n^T(\theta_q, \phi_q) \mathbf{s}'_1(k + \Delta) + v_n(k), \quad (6)$$

where $\mathbf{s}'_1(k + \Delta)$ is a vector comprising L_q samples of $s_1(k)$ and $\mathbf{r}_n(\theta_q, \phi_q)$ are finite impulse response approximations, which functionally depend on the direction of the desired source. Vectors $\mathbf{s}'_1(k + \Delta)$ and $\mathbf{r}_n(\theta_q, \phi_q)$ are expressed as

$$\begin{aligned} \mathbf{s}'_1(k + \Delta) &= \\ [s_1(k + \Delta) \quad s_1(k + \Delta - 1) \quad \dots \quad s_1(k + \Delta - L_q + 1)]^T, \\ \mathbf{r}_n(\theta_q, \phi_q) &= \\ [r_n(-\Delta) \quad r_n(1 - \Delta) \quad \dots \quad r_n(L_q - 1 - \Delta)]^T. \end{aligned} \quad (7)$$

The relative impulse response of the reference sensor is explicitly given by

$$\mathbf{r}_1(\theta_q, \phi_q) = [0 \quad \dots \quad 0 \quad 1 \quad 0 \quad \dots \quad 0]^T, \quad (9)$$

where the $(\Delta + 1)$ th component of $\mathbf{r}_1(\theta_q, \phi_q)$ is 1.

Considering L_u time samples of the observation signal from the n th sensor, we obtain:

$$\begin{aligned} \mathbf{u}_n(k) &= [u_n(k) \quad u_n(k - 1) \quad \dots \quad u_n(k - L_u + 1)]^T \\ &= \mathbf{R}_n(\theta_q, \phi_q) \bar{\mathbf{s}}_1(k + \Delta) + \mathbf{v}_n(k) \\ &= \mathbf{s}_n(k) + \mathbf{v}_n(k), \end{aligned} \quad (10)$$

where $\mathbf{R}_n(\theta_q, \phi_q)$ is a Toeplitz matrix of dimension $L_u \times L$, $L = L_q + L_u - 1$, and $\bar{\mathbf{s}}_1(k + \Delta)$ is a vector containing L samples of $s_1(k)$. The matrix $\mathbf{R}_n(\theta_q, \phi_q)$ and vector $\bar{\mathbf{s}}_1(k + \Delta)$ are given by

$$\begin{aligned} \mathbf{R}_n(\theta_q, \phi_q) &= \\ \begin{bmatrix} \mathbf{r}_n^T(\theta_q, \phi_q) & 0 & 0 & \dots & 0 \\ 0 & \mathbf{r}_n^T(\theta_q, \phi_q) & 0 & \dots & 0 \\ \vdots & \vdots & \ddots & \ddots & \vdots \\ 0 & 0 & 0 & \dots & \mathbf{r}_n^T(\theta_q, \phi_q) \end{bmatrix}, \end{aligned} \quad (11)$$

$$\begin{aligned} \bar{\mathbf{s}}_1(k + \Delta) &= \\ [s_1(k + \Delta) \quad s_1(k + \Delta - 1) \quad \dots \quad s_1(k + \Delta - L + 1)]^T, \end{aligned} \quad (12)$$

and the vectors $\mathbf{s}_n(k)$ and $\mathbf{v}_n(k)$, of length L_u , are given by

$$\begin{aligned} \mathbf{s}_n(k) &= [s_n(k) \quad s_n(k - 1) \quad \dots \quad s_n(k - L_u + 1)]^T \\ &= \mathbf{R}_n(\theta_q, \phi_q) \bar{\mathbf{s}}_1(k + \Delta), \\ \mathbf{v}_n(k) &= [v_n(k) \quad v_n(k - 1) \quad \dots \quad v_n(k - L_u + 1)]^T. \end{aligned} \quad (13)$$

The observation signals from the N sensors are concatenated to obtain the vector $\mathbf{u}(k)$, of length NL_u , expressed as

$$\mathbf{u}(k) = [\mathbf{u}_1^T(k) \quad \mathbf{u}_2^T(k) \quad \dots \quad \mathbf{u}_N^T(k)]^T$$

$$\begin{aligned} &= \mathbf{R}(\theta_q, \phi_q) \bar{\mathbf{s}}_1(k + \Delta) + \mathbf{v}(k) \\ &= \mathbf{s}(k) + \mathbf{v}(k), \end{aligned} \quad (15)$$

where $\mathbf{R}(\theta_q, \phi_q)$ is the relative impulse response matrix of dimension $NL_u \times L$,

$$\mathbf{R}(\theta_q, \phi_q) = \begin{bmatrix} \mathbf{R}_1(\theta_q, \phi_q) \\ \mathbf{R}_2(\theta_q, \phi_q) \\ \vdots \\ \mathbf{R}_N(\theta_q, \phi_q) \end{bmatrix}, \quad (16)$$

and $\mathbf{s}(k)$ and $\mathbf{v}(k)$ are concatenated vectors of length NL_u ,

$$\begin{aligned} \mathbf{s}(k) &= [\mathbf{s}_1^T(k) \quad \mathbf{s}_2^T(k) \quad \dots \quad \mathbf{s}_N^T(k)]^T \\ &= \mathbf{R}(\theta_q, \phi_q) \bar{\mathbf{s}}_1(k + \Delta), \\ \mathbf{v}(k) &= [\mathbf{v}_1^T(k) \quad \mathbf{v}_2^T(k) \quad \dots \quad \mathbf{v}_N^T(k)]^T. \end{aligned} \quad (17)$$

From (15), the covariance matrix of $\mathbf{u}(k)$, of dimension $NL_u \times NL_u$, is obtained as follows:

$$\begin{aligned} \mathbf{C}_{\mathbf{u}} &= \mathbb{E}[\mathbf{u}(k)\mathbf{u}^T(k)] \\ &= \mathbf{C}_{\mathbf{s}} + \mathbf{C}_{\mathbf{v}} \\ &= \mathbf{R}(\theta_q, \phi_q) \mathbf{C}_{\bar{\mathbf{s}}_1} \mathbf{R}^T(\theta_q, \phi_q) + \mathbf{C}_{\mathbf{v}}, \end{aligned} \quad (18)$$

where $\mathbf{C}_{\bar{\mathbf{s}}_1}$, $\mathbf{C}_{\mathbf{s}}$, and $\mathbf{C}_{\mathbf{v}}$ are the covariance matrices of $\bar{\mathbf{s}}_1(k + \Delta)$, $\mathbf{s}(k)$, and $\mathbf{v}(k)$, respectively. The output of the beamformer can be obtained using a real-valued spatiotemporal filter and is given by

$$\begin{aligned} y(k) &= \sum_{n=1}^N \mathbf{g}_n^T \mathbf{u}_n(k) \\ &= \mathbf{g}^T \mathbf{u}(k) \\ &= s_{fd}(k) + v_m(k), \end{aligned} \quad (19)$$

where $\mathbf{g} = [\mathbf{g}_1^T \quad \mathbf{g}_2^T \quad \dots \quad \mathbf{g}_N^T]^T$ is the beamformer weights of length NL_u , \mathbf{g}_n is the temporal filter of the n th sensor of length L_u , $s_{fd}(k)$ is the filtered desired signal, and $v_m(k)$ is the residual noise. The signals $s_{fd}(k)$ and $v_m(k)$ are expressed as

$$\begin{aligned} s_{fd}(k) &= \sum_{n=1}^N \mathbf{g}_n^T \mathbf{r}_n(\theta_q, \phi_q) \bar{\mathbf{s}}_1(k + \Delta) \\ &= \mathbf{g}^T \mathbf{R}(\theta_q, \phi_q) \bar{\mathbf{s}}_1(k + \Delta), \end{aligned} \quad (20)$$

$$\begin{aligned} v_m(k) &= \sum_{n=1}^N \mathbf{g}_n^T \mathbf{v}_n(k) \\ &= \mathbf{g}^T \mathbf{v}(k). \end{aligned} \quad (21)$$

A. GSC Beamformer

The conventional GSC beamformer is designed to optimize the beamforming weights for a single target direction (θ_q, ϕ_q) . The objective is to enhance the signal that arrives from this specified direction, while suppressing interference and noise originating from all other directions. To achieve this, the beamforming weight vector is decomposed into two components: one

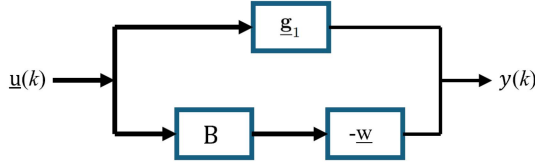


Fig. 1. Framework of the conventional generalized sidelobe canceller (GSC). The GSC beamformer consists of data-independent beamformer weights $\underline{\mathbf{g}}_1$, a blocking matrix \mathbf{B} , and data-dependent beamformer weights $\underline{\mathbf{w}}$.

that aligns with the signal subspace associated with the specified direction and another that lies in its null space. The beamformer for a single target direction is obtained by minimizing the output power $\underline{\mathbf{g}}^T \Gamma_{\mathbf{v}} \underline{\mathbf{g}}$ subject to the constraint $\underline{\mathbf{g}}^T \mathbf{R}(\theta_q, \phi_q) = \mathbf{i}_l^T$, resulting in the constrained optimization problem:

$$\min_{\underline{\mathbf{g}}} \underline{\mathbf{g}}^T \Gamma_{\mathbf{v}} \underline{\mathbf{g}} \quad \text{subject to} \quad \Gamma_{\mathbf{R}} \underline{\mathbf{g}} = \mathbf{R} \mathbf{i}_l. \quad (22)$$

where \mathbf{i}_l is the l th column of the identity matrix I_L of dimension $L \times L$. From (20) and (22), it can be observed that any element of the vector $\bar{\mathbf{s}}_1(k + \Delta)$ can be treated as the desired signal by choosing a corresponding value for l . For a specific direction (θ, ϕ) , $\Gamma_{\mathbf{R}}$ can be expressed as

$$\Gamma_{\mathbf{R}} = \mathbf{R}(\theta, \phi) \mathbf{R}^T(\theta, \phi). \quad (23)$$

The problem defined in (22) can be reformulated in the unconstrained GSC framework. As illustrated in Fig. 1, the weight vector is decomposed into two components $\underline{\mathbf{g}} = \underline{\mathbf{g}}_1 + \underline{\mathbf{g}}_2$. The optimization problem for the GSC beamformer can be formulated as:

$$\min_{\underline{\mathbf{w}}} (\underline{\mathbf{g}}_1 - \mathbf{B} \underline{\mathbf{w}})^T \Gamma_{\mathbf{v}} (\underline{\mathbf{g}}_1 - \mathbf{B} \underline{\mathbf{w}}), \quad (24)$$

where $\underline{\mathbf{g}}_1$ is the data-independent beamformer weights obtained for a single direction, $\underline{\mathbf{g}}_2 = -\mathbf{B} \underline{\mathbf{w}}$ is the data-dependent beamformer weights, and \mathbf{B} is the blocking matrix corresponding to the single target direction. Here, $\underline{\mathbf{g}}_1$ is the minimum-norm solution to the constraint $\mathbf{R}^T(\theta, \phi) \underline{\mathbf{g}}_1 = \mathbf{i}_l$. The matrix $\Gamma_{\mathbf{v}}$ is the pseudo-correlation matrix of $\underline{\mathbf{v}}(k)$, given by

$$\Gamma_{\mathbf{v}} = \frac{\mathbf{C}_{\mathbf{v}}}{\sigma_{v_1}^2}, \quad (25)$$

where $\sigma_{v_1}^2$ denotes the variance of the signal $v_1(k)$. The solution to (24) is expressed as

$$\underline{\mathbf{w}} = [\mathbf{B}^T \Gamma_{\mathbf{v}} \mathbf{B}]^{-1} \mathbf{B}^T \Gamma_{\mathbf{v}} \underline{\mathbf{g}}_1. \quad (26)$$

This formulation enables focused signal enhancement in a single spatial direction. However, it is inherently limited to static scenarios and may underperform when there is movement of either the source or the array. To overcome this limitation, the ROI-based GSC beamformer extends the optimization framework to consider a set of directions defined by the ROI simultaneously.

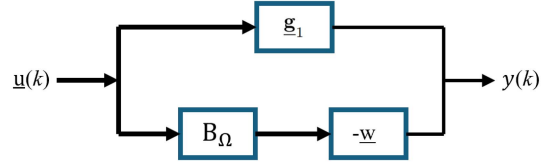


Fig. 2. Framework of the region-of-interest (ROI) GSC. The ROI-GSC beamformer consists of data-independent beamformer weights $\underline{\mathbf{g}}_1$, a ROI blocking matrix \mathbf{B}_{Ω} , and data-dependent beamformer weights $\underline{\mathbf{w}}$.

III. PROPOSED METHODOLOGY

The main objective of this study is to design an optimal time-domain broadband GSC beamformer tailored for a specified ROI, Ω . The set Ω represents all the angular directions towards the ROI. This section explores the derivation of optimal time-domain convolutive filters for ROI beamforming within the GSC framework.

A. ROI-GSC Beamformer

To design the proposed beamformer, we aim to minimize the average distortion over the ROI, which is defined as

$$J_{q,\Omega}(\underline{\mathbf{g}}) = \frac{1}{|\Omega|} \iint_{(\theta,\phi) \in \Omega} \mathbf{H}^T \mathbf{H} \sin \theta d\phi d\theta, \quad (27)$$

where $\mathbf{H} = \mathbf{R}^T(\theta, \phi) \underline{\mathbf{g}} - \mathbf{i}_l$ and $|\Omega| = \iint_{(\theta,\phi) \in \Omega} \sin \theta d\phi d\theta$. Expanding $J_{q,\Omega}(\underline{\mathbf{g}})$ in (27) yields the quadratic form:

$$J_{q,\Omega}(\underline{\mathbf{g}}) = \underline{\mathbf{g}}^T \Gamma_{\mathbf{R},\Omega} \underline{\mathbf{g}} - \underline{\mathbf{g}}^T \mathbf{R}_{\Omega} \mathbf{i}_l - \mathbf{i}_l^T \mathbf{R}_{\Omega}^T \underline{\mathbf{g}} + 1, \quad (28)$$

where

$$\mathbf{R}_{\Omega} = \frac{1}{|\Omega|} \iint_{(\theta,\phi) \in \Omega} \mathbf{R}(\theta, \phi) \sin \theta d\phi d\theta, \quad (29)$$

and

$$\Gamma_{\mathbf{R},\Omega} = \frac{1}{|\Omega|} \iint_{(\theta,\phi) \in \Omega} \mathbf{R}(\theta, \phi) \mathbf{R}^T(\theta, \phi) \sin \theta d\phi d\theta. \quad (30)$$

To minimize the distortion over the ROI, we take the gradient of (28) with respect to $\underline{\mathbf{g}}$ and equate it to zero, yielding:

$$\Gamma_{\mathbf{R},\Omega} \underline{\mathbf{g}} = \mathbf{R}_{\Omega} \mathbf{i}_l. \quad (31)$$

The ROI beamformer is obtained by minimizing the output power $\underline{\mathbf{g}}^T \Gamma_{\mathbf{v}} \underline{\mathbf{g}}$ subject to the constraint in (31), resulting in the constrained optimization problem:

$$\min_{\underline{\mathbf{g}}} \underline{\mathbf{g}}^T \Gamma_{\mathbf{v}} \underline{\mathbf{g}} \quad \text{subject to} \quad \Gamma_{\mathbf{R},\Omega} \underline{\mathbf{g}} = \mathbf{R}_{\Omega} \mathbf{i}_l. \quad (32)$$

This problem can be reformulated in the unconstrained GSC framework. As illustrated in Fig. 2, the weight vector is decomposed into two components $\underline{\mathbf{g}} = \underline{\mathbf{g}}_1 + \underline{\mathbf{g}}_2$, and the problem is formulated as

$$\min_{\underline{\mathbf{w}}} (\underline{\mathbf{g}}_1 - \mathbf{B}_{\Omega} \underline{\mathbf{w}})^T \Gamma_{\mathbf{v}} (\underline{\mathbf{g}}_1 - \mathbf{B}_{\Omega} \underline{\mathbf{w}}), \quad (33)$$

where $\underline{\mathbf{g}}_1$ is the data-independent beamformer weights designed for ROI, $\underline{\mathbf{g}}_2 = -\mathbf{B}_{\Omega} \underline{\mathbf{w}}$ is the data-dependent beamformer weights, and \mathbf{B}_{Ω} is the blocking matrix corresponding to the

ROI. The construction of \mathbf{B}_Ω is discussed in the next subsection. The solution to (33) is given as

$$\underline{\mathbf{w}} = [\mathbf{B}_\Omega^T \Gamma_{\underline{\mathbf{v}}} \mathbf{B}_\Omega]^{-1} \mathbf{B}_\Omega^T \Gamma_{\underline{\mathbf{v}}} \underline{\mathbf{g}}_1. \quad (34)$$

In the following discussion, we outline the procedure for determining the data-independent beamformer weights, $\underline{\mathbf{g}}_1$, which are computed for an ROI without relying on specific input data. These weights are derived by utilizing the matrix $\Gamma_{\mathbf{R},\Omega}$, its diagonalization, and the corresponding signal subspace. This subspace is constructed using the most significant components of $\Gamma_{\mathbf{R},\Omega}$, corresponding to its largest eigenvalues. These components capture the characteristics of the desired signal subspace, and they form the basis for calculating the beamformer weights $\underline{\mathbf{g}}_1$. In this problem formulation, we assume that the rank of $\Gamma_{\mathbf{R},\Omega}$ is $R < NL_u$ and that the matrix $\Gamma_{\underline{\mathbf{v}}}$ is full-rank. The matrix $\Gamma_{\mathbf{R},\Omega}$ is diagonalized to obtain:

$$\underline{\mathbf{T}}^T \Gamma_{\mathbf{R},\Omega} \underline{\mathbf{T}} = \underline{\mathbf{\Lambda}}, \quad (35)$$

where

$$\underline{\mathbf{T}} = [\underline{\mathbf{t}}_1 \quad \underline{\mathbf{t}}_2 \quad \cdots \quad \underline{\mathbf{t}}_{NL_u}] \quad (36)$$

is a matrix of dimension $NL_u \times NL_u$, where the columns of the matrix correspond to the eigenvectors and the diagonal matrix

$$\underline{\mathbf{\Lambda}} = \text{diag}(\lambda_1, \lambda_2, \dots, \lambda_{NL_u}) \quad (37)$$

contains the corresponding real eigenvalues, ordered such that $\lambda_1 \geq \lambda_2 \geq \cdots \geq \lambda_R > \lambda_{R+1} = \cdots = \lambda_{NL_u} = 0$, and their corresponding eigenvectors are $\underline{\mathbf{t}}_1, \underline{\mathbf{t}}_2, \dots, \underline{\mathbf{t}}_{NL_u}$, respectively. The matrix $\underline{\mathbf{T}}$ can be written as follows:

$$\underline{\mathbf{T}} = [\underline{\mathbf{T}}_1 \quad \underline{\mathbf{T}}_2], \quad (38)$$

where $\underline{\mathbf{T}}_1$ is the matrix having dimension $NL_u \times R$ that contains the eigenvectors corresponding to the signal subspace and $\underline{\mathbf{T}}_2$ is the matrix having dimension $NL_u \times (NL_u - R)$ that contains the eigenvectors corresponding to the noise subspace. The weight vector of the beamformer $\underline{\mathbf{g}}_1$ can be decomposed into the following:

$$\begin{aligned} \underline{\mathbf{g}}_1 &= \underline{\mathbf{T}} \underline{\mathbf{a}} \\ &= \underline{\mathbf{T}}_1 \underline{\mathbf{a}}_1 + \underline{\mathbf{T}}_2 \underline{\mathbf{a}}_2, \end{aligned} \quad (39)$$

where $\underline{\mathbf{a}} = [\underline{\mathbf{a}}_1^T \quad \underline{\mathbf{a}}_2^T]^T$ is the transformed weight vector. The constraint in (31) corresponding to the signal subspace can be written as

$$\underline{\mathbf{\Lambda}}_1 \underline{\mathbf{a}}_1 = \underline{\mathbf{T}}_1^T \mathbf{R}_\Omega \mathbf{i}_l. \quad (40)$$

The transformed weight vector corresponding to the signal subspace can be expressed as follows:

$$\underline{\mathbf{a}}_1 = \underline{\mathbf{\Lambda}}_1^{-1} \underline{\mathbf{T}}_1^T \mathbf{R}_\Omega \mathbf{i}_l. \quad (41)$$

The eigenvectors corresponding to the largest eigenvalues spanning the signal subspace capture the dominant components of the relative impulse responses within the ROI, where $\underline{\mathbf{g}}_1$ is expressed in the eigenbasis mentioned in (39). By selecting $\underline{\mathbf{a}}_1$ as in (41), we ensure that $\underline{\mathbf{g}}_1$ is within the signal subspace and satisfies the minimum distortion constraint in (31). Therefore, (39) provides a constructive procedure to obtain $\underline{\mathbf{g}}_1$ that enforces

unity response averaged over the ROI. In summary, the design criterion for $\underline{\mathbf{g}}_1$ is to minimize the distortion across the ROI. (39) fulfills this requirement by explicitly constraining $\underline{\mathbf{g}}_1$ to the ROI signal subspace, thereby preserving the desired signal components while leaving the adaptive part of the GSC to mitigate residual interference and noise. The data-independent beamformer weights that correspond to the signal subspace can be obtained using (41) and are given by

$$\begin{aligned} \underline{\mathbf{g}}_1 &= \underline{\mathbf{T}}_1 \underline{\mathbf{a}}_1 \\ &= \underline{\mathbf{T}}_1 \underline{\mathbf{\Lambda}}_1^{-1} \underline{\mathbf{T}}_1^T \mathbf{R}_\Omega \mathbf{i}_l \\ &= \left[\sum_{r=1}^R \frac{\underline{\mathbf{t}}_r \underline{\mathbf{t}}_r^T}{\lambda_r} \right] \mathbf{R}_\Omega \mathbf{i}_l. \end{aligned} \quad (42)$$

The weight vector $\underline{\mathbf{g}}_1$ and \mathbf{B}_Ω are fixed, and the component $\underline{\mathbf{w}}$ is set to minimize the output power of the GSC beamformer. The data-dependent beamformer weights can be obtained using (34) and are given as follows:

$$\underline{\mathbf{g}}_2 = -\mathbf{B}_\Omega [\mathbf{B}_\Omega^T \Gamma_{\underline{\mathbf{v}}} \mathbf{B}_\Omega]^{-1} \mathbf{B}_\Omega^T \Gamma_{\underline{\mathbf{v}}} \underline{\mathbf{g}}_1. \quad (43)$$

The final weights of the proposed ROI-GSC beamformer can be obtained as $\underline{\mathbf{g}} = \underline{\mathbf{g}}_1 + \underline{\mathbf{g}}_2$. To improve the robustness of the proposed beamformer, we modify the expression in (42) so that it is expressed as follows:

$$\underline{\mathbf{g}}_{1\mathcal{L},\mu} = \left[\sum_{r=1}^{\mathcal{L}} \frac{\underline{\mathbf{t}}_r \underline{\mathbf{t}}_r^T}{\lambda_r + \mu \lambda_1} \right] \mathbf{R}_\Omega \mathbf{i}_l, \quad (44)$$

where $1 \leq \mathcal{L} \leq R$, $\mu \geq 0$, and $\mu \lambda_1$ is the regularization term. The parameter μ is selected based on the noise level or by empirical methods.

B. Design of the ROI Blocking Matrix

This section presents two methods for constructing a blocking matrix for the ROI-GSC beamformer.

1) *Blocking Matrix 1*: The eigenspace blocking matrix is used as a projection matrix onto the null space of the constraint matrix, as detailed in [1]. It is designed to project signals that do not correspond to the desired direction. This matrix essentially blocks the components of the incoming signals arriving from the direction of interest, ensuring that only unwanted noise or interference is passed through while the desired signals are blocked. For a signal arriving from a specific direction (θ, ϕ) , the blocking matrix \mathbf{B} can be expressed as

$$\mathbf{B} = \mathbf{I}_{NL_u} - \mathbf{R}(\theta, \phi) [\mathbf{R}(\theta, \phi)^T \mathbf{R}(\theta, \phi)]^{-1} \mathbf{R}(\theta, \phi)^T, \quad (45)$$

where \mathbf{I}_{NL_u} represents the identity matrix of dimension $NL_u \times NL_u$.

The same principles apply to obtain the eigenspace blocking matrix corresponding to the ROI. The matrix is computed to block signals arriving from the specific spatial region Ω , effectively isolating the desired sources within that region while allowing signals from other areas to pass through. We can obtain an eigenspace blocking matrix corresponding to an ROI as

follows:

$$\mathbf{B}_\Omega = \mathbf{I}_{NL_u} - \mathbf{R}_\Omega [\mathbf{R}_\Omega^T \mathbf{R}_\Omega]^{-1} \mathbf{R}_\Omega^T. \quad (46)$$

2) *Blocking Matrix 2*: The design of the blocking matrix 2 is based on the eigen-decomposition of the spatial correlation matrix $\mathbf{\Gamma}_{\mathbf{R},\Omega}$, which captures the spatial-temporal structure of the received signals in the ROI. The first \mathcal{L} dominant eigenvectors span the signal subspace representing the components most strongly aligned with the desired signal directions. These eigenvectors effectively capture the relative impulse responses of the target signals across the sensor array in the time domain. The remaining eigenvectors span the noise and interference subspace, which is orthogonal to the desired signal subspace. By construction, this orthogonality enables us to isolate the interference and noise components while removing the direct contributions from the ROI. The blocking matrix is therefore constructed from this noise subspace. Formally, the blocking matrix $\mathbf{B}_{\Omega\mathcal{L},\mu}$ is expressed as:

$$\mathbf{B}_{\Omega\mathcal{L},\mu} = \left[\sum_{r=\mathcal{L}+1}^{NL_u} \frac{\mathbf{t}_r \mathbf{t}_r^T}{\lambda_r + \mu\lambda_1} \right]. \quad (47)$$

The denominator includes a regularization term $\mu\lambda_1$, scaled by the largest eigenvalue, which stabilizes the computation and prevents numerical issues arising from very small or near-zero eigenvalues. Intuitively, this construction ensures that the blocking matrix projects the received signals onto the subspace that is orthogonal to the ROI signal components. As a result, the desired signal is effectively suppressed, while the residual contains only interference and noise contributions. By leveraging the relative impulse response structure present in $\mathbf{\Gamma}_{\mathbf{R},\Omega}$, this design explicitly accounts for time-domain propagation effects. In summary, the blocking matrix $\mathbf{B}_{\Omega\mathcal{L},\mu}$ is carefully derived from the noise subspace of $\mathbf{\Gamma}_{\mathbf{R},\Omega}$, ensuring that the ROI components are nulled while preserving robustness. This provides a mathematically grounded way to incorporate relative impulse responses in the time-domain ROI-GSC framework. In this work, the fixed beamformer \mathbf{g}_1 is constructed from the signal subspace of $\mathbf{\Gamma}_{\mathbf{R},\Omega}$, while the blocking matrix is obtained from its complementary noise subspace. This joint design ensures that the beamformer achieves minimum distortion over the ROI and that the blocking matrix preserves orthogonality with respect to the ROI signal components. As a result, alternative approaches, such as widening the main lobe of a conventional beamformer, cannot be incorporated into this framework, since they would not satisfy the required subspace structure. The works [54], [55] explore methods to enhance the robustness of the beamformer, in which controlling the WNG and the directivity factor (DF) is discussed. Therefore, to enhance the robustness of the proposed ROI-GSC beamformer and achieve a balance between noise reduction, DF, and WNG, we replace $\mathbf{\Gamma}_{\mathbf{v}}$ in (43) with $\mathbf{\Gamma}_{\mathbf{v},\epsilon}$, which is expressed as

$$\mathbf{\Gamma}_{\mathbf{v},\epsilon} = (1 - \epsilon_0 - \epsilon_1) \mathbf{\Gamma}_{\mathbf{v}} + \epsilon_0 \mathbf{\Gamma}_0 + \epsilon_1 \mathbf{I}_{NL_u}, \quad (48)$$

where $0 \leq \epsilon_0 \leq 1$ and $0 \leq \epsilon_1 \leq 1 - \epsilon_0$ are the parameters that balance the tradeoff between noise reduction, WNG, and DF. The inclusion of ϵ_0 and ϵ_1 allows the beamformer to operate

effectively in diverse acoustic conditions, such as reverberant environments or scenarios with sensor noise. Here, $\mathbf{\Gamma}_0$ is the pseudo-correlation matrix of diffuse noise and \mathbf{I}_{NL_u} is the pseudo-correlation matrix of the white noise. The pseudo-correlation matrix $\mathbf{\Gamma}_{\mathbf{v},\epsilon}$ is a matrix of dimension $NL_u \times NL_u$ that represents a weighted combination of the pseudo-correlation matrices of the noise signal, diffuse noise, and white noise. Therefore, we replace the data-independent beamformer weights in (43) with:

$$\mathbf{g}_{2\mathcal{L},\mu,\epsilon} = -\mathbf{B}_{\Omega\mathcal{L},\mu} [\mathbf{B}_{\Omega\mathcal{L},\mu}^T \mathbf{\Gamma}_{\mathbf{v},\epsilon} \mathbf{B}_{\Omega\mathcal{L},\mu}]^{-1} \mathbf{B}_{\Omega\mathcal{L},\mu}^T \mathbf{\Gamma}_{\mathbf{v},\epsilon} \mathbf{g}_1. \quad (49)$$

The maximum value of the average gain of the ROI beamformer is obtained when $\mathcal{L} = 1$, and the weights expressed in (44) can be replaced as follows for $\mathcal{L} = 1$:

$$\mathbf{g}_{11,0} = \frac{\mathbf{t}_1 \mathbf{t}_1^T}{\lambda_1} \mathbf{R}_\Omega \mathbf{i}_1. \quad (50)$$

The weights expressed in (49) for $\mathcal{L} = 1$ and $\epsilon_1 = \epsilon_0 = 0$ can be expressed as follows:

$$\mathbf{g}_{21,\mu,0} = -\mathbf{B}_{\Omega 1,\mu} [\mathbf{B}_{\Omega 1,\mu}^T \mathbf{\Gamma}_{\mathbf{v},\epsilon} \mathbf{B}_{\Omega 1,\mu}]^{-1} \mathbf{B}_{\Omega 1,\mu}^T \mathbf{\Gamma}_{\mathbf{v},\epsilon} \mathbf{g}_1. \quad (51)$$

The final weights of the proposed beamformer for $\mathcal{L} = 1$ can be obtained as

$$\mathbf{g} = \mathbf{g}_{11,0} + \mathbf{g}_{21,\mu,0}. \quad (52)$$

Although this configuration provides the maximum average array gain over the ROI, it results in increased signal distortion. Decreasing the value of \mathcal{L} enhances the average array gain over the ROI but also leads to higher signal distortion.

C. ROI RLS-GSC Beamformer

This section presents an adaptive implementation of the ROI-GSC beamformer using the RLS algorithm. The main advantage of the RLS approach is its ability to adapt the beamforming weights in response to non-stationary noise dynamically. In contrast to traditional batch methods, which require the recomputation of optimal weights whenever the noise characteristics change, the RLS algorithm updates the weights continuously using incoming data. This allows the beamformer to maintain effective noise suppression even under non-stationary conditions.

The RLS algorithm estimates the mean squared error (MSE) using a weighted least squares approach, where the cost function is defined as $J[\mathbf{w}(k)] = \sum_{n=1}^k \beta^{k-n} e^2(n)$, where β is the forgetting factor. The ROI RLS-GSC beamformer framework is shown in Fig. 3. The weight update equations of the ROI-GSC implementation using RLS are given as follows:

$$\mathbf{u}_{\text{GSC}}(k) = \mathbf{B}_{\Omega}^T \mathbf{u}(k), \quad (53)$$

$$e(k) = \mathbf{g}_{1R,\mu}^T \mathbf{u}(k) - \mathbf{w}^T(k) \mathbf{u}_{\text{GSC}}(k), \quad (54)$$

$$\mathbf{h}_{\text{GSC}}(k) = \frac{\mathbf{C}_{\text{GSC}}^{-1}(k) \mathbf{u}_{\text{GSC}}(k)}{\beta + \mathbf{u}_{\text{GSC}}^T(k) \mathbf{C}_{\text{GSC}}^{-1}(k) \mathbf{u}_{\text{GSC}}(k)}, \quad (55)$$

$$\mathbf{w}(k) = \mathbf{w}(k-1) + e(k) \mathbf{h}_{\text{GSC}}(k), \quad (56)$$

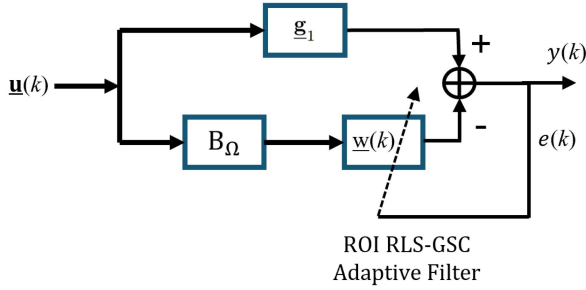


Fig. 3. Framework of the ROI RLS-GSC. The weight vector $\underline{\mathbf{w}}(k)$ is adaptive and is updated using the error signal $e(k)$.

where $\underline{\mathbf{u}}_{\text{GSC}}(k)$ is the input to the adaptive filter, $e(k)$ is the error of the adaptive filter, and $\mathbf{C}_{\text{GSC}}(k) = \underline{\mathbf{u}}_{\text{GSC}}(k)\underline{\mathbf{u}}_{\text{GSC}}^T(k)$ is the covariance matrix of the input signal to the adaptive filter. The inverse of the correlation matrix $\mathbf{C}_{\text{GSC}}(k)$ can be updated recursively using the standard matrix inversion lemma, which is expressed as follows:

$$\mathbf{C}_{\text{GSC}}^{-1}(k) = \frac{\mathbf{C}_{\text{GSC}}^{-1}(k-1)}{\beta} [1 - \mathbf{h}_{\text{GSC}}(k)\underline{\mathbf{u}}_{\text{GSC}}^T(k)], \quad (57)$$

where $0 < \beta < 1$ is the forgetting factor.

D. ROI LMS-GSC Beamformer

In this section, we derive the optimal weight formulation based on the ROI design. The objective function to be minimized corresponds to the mean-squared error of the LMS-GSC beamformer in the ROI setting, which is given by:

$$J(\underline{\mathbf{w}}) = \mathbb{E}\left\{|d(k) - \underline{\mathbf{w}}^T \underline{\mathbf{u}}_{\text{GSC}}(k)|^2\right\} \quad (58)$$

where $d(k)$ is the output signal of the data-independent beamformer filter. Equation (58) can be expanded as follows:

$$\begin{aligned} J(\underline{\mathbf{w}}) &= \mathbb{E}\{|d(k)|^2\} - \mathbb{E}\{\underline{\mathbf{w}}^T \underline{\mathbf{u}}_{\text{GSC}}(k)d(k)\} \\ &\quad - \mathbb{E}\{d(k)\underline{\mathbf{u}}_{\text{GSC}}^T(k)\underline{\mathbf{w}}\} \\ &\quad + \mathbb{E}\{\underline{\mathbf{w}}^T \underline{\mathbf{u}}_{\text{GSC}}(k)\underline{\mathbf{u}}_{\text{GSC}}^T(k)\underline{\mathbf{w}}\} \\ &= \mathbf{g}_{1R,\mu}^T \mathbf{C}_{\underline{\mathbf{u}}}\mathbf{g}_{1R,\mu} - 2\underline{\mathbf{w}}^T \mathbf{p}_{\Omega} + \underline{\mathbf{w}}^T \mathbf{C}_{\text{GSC}}\underline{\mathbf{w}}. \end{aligned} \quad (59)$$

where $\mathbf{p}_{\Omega} \triangleq \mathbb{E}\{\underline{\mathbf{u}}_{\text{GSC}}(k)d(k)\}$ is the cross-correlation vector and $\mathbf{C}_{\text{GSC}} \triangleq \mathbb{E}\{\underline{\mathbf{u}}_{\text{GSC}}(k)\underline{\mathbf{u}}_{\text{GSC}}^T(k)\}$ is the covariance matrix. To obtain the optimal Wiener solution, we minimize $J(\underline{\mathbf{w}})$ by setting the gradient with respect to $\underline{\mathbf{w}}$ to zero:

$$\frac{\partial J(\underline{\mathbf{w}})}{\partial \underline{\mathbf{w}}} = -\mathbf{p}_{\Omega} + \mathbf{C}_{\text{GSC}}\underline{\mathbf{w}} = 0. \quad (60)$$

Solving for $\underline{\mathbf{w}}$ yields

$$\underline{\mathbf{w}}_{\text{opt},\Omega} = \mathbf{C}_{\text{GSC}}^{-1}\mathbf{p}_{\Omega} = (\mathbf{B}_{\Omega}^T \mathbf{C}_{\underline{\mathbf{u}}}\mathbf{B}_{\Omega})^{-1} \mathbf{B}_{\Omega}^T \mathbf{C}_{\underline{\mathbf{u}}}\mathbf{g}_{1R,\mu}, \quad (61)$$

where $\underline{\mathbf{w}}_{\text{opt},\Omega}$ denotes the optimal Wiener solution. While the optimal Wiener solution provides the closed-form optimal weight vector that minimizes the mean-squared error, its computation requires knowledge of the second-order statistics, i.e., \mathbf{C}_{GSC} and \mathbf{p}_{Ω} . In practice, these quantities are not available a priori and

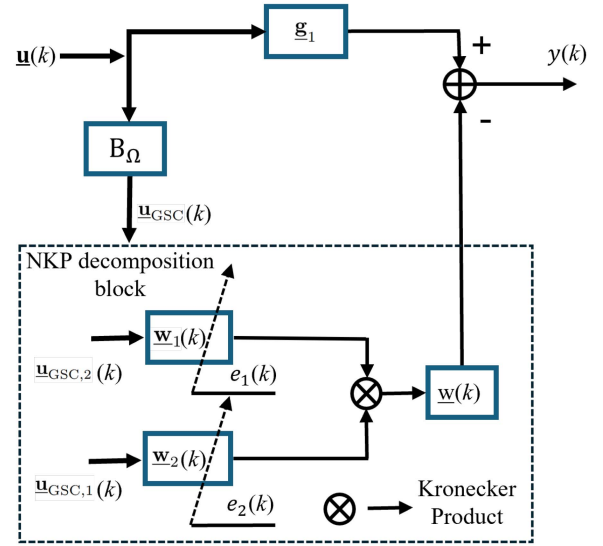


Fig. 4. Framework of the ROI NKP RLS-GSC. The NKP decomposition block comprises two adaptive filters with weights $\underline{\mathbf{w}}_1(k)$ and $\underline{\mathbf{w}}_2(k)$, which are updated adaptively based on the respective errors $e_1(k)$ and $e_2(k)$.

must be estimated from data. The LMS algorithm addresses this limitation by iteratively updating the weight vector using instantaneous samples of the error and input, thereby providing a low-complexity stochastic gradient approximation to the Wiener solution. As a result, the ROI LMS-GSC beamformer converges asymptotically to the optimal weight.

The LMS approach, unlike RLS, offers a simpler and computationally efficient update rule. However, LMS generally converges more slowly than RLS. The cost function minimized by LMS is

$$J[\underline{\mathbf{w}}(k)] = \mathbb{E}\{e^2(k)\}, \quad (62)$$

where $e(k)$ is the error of the adaptive filter. The update equations of the ROI-GSC implementation using LMS are given as follows:

$$\underline{\mathbf{u}}_{\text{GSC}}(k) = \mathbf{B}_{\Omega}^T \underline{\mathbf{u}}(k), \quad (63)$$

$$e(k) = \mathbf{g}_{1R,\mu}^T \underline{\mathbf{u}}(k) - \underline{\mathbf{w}}^T(k)\underline{\mathbf{u}}_{\text{GSC}}(k), \quad (64)$$

$$\underline{\mathbf{w}}(k) = \underline{\mathbf{w}}(k-1) + \mu e(k)\underline{\mathbf{u}}_{\text{GSC}}(k), \quad (65)$$

where $0 < \mu < \frac{2}{\underline{\mathbf{u}}_{\text{GSC}}^T(k)\underline{\mathbf{u}}_{\text{GSC}}(k)}$ is the step size parameter that controls the convergence.

E. ROI NKP RLS-GSC Beamformer

This section presents an adaptive ROI-GSC beamformer that incorporates NKP decomposition of the weight vector $\underline{\mathbf{w}}$ within the RLS framework. The structure of the proposed ROI adaptive beamformer is shown in Fig. 4. The key advantage of this method is its reduced computational complexity compared to conventional full-rank updates. The update rules for the decomposed ROI-GSC weight vectors can be derived using the identity $\underline{\mathbf{w}}_{2,r} \otimes \underline{\mathbf{w}}_{1,r} = (\underline{\mathbf{w}}_{2,r} \otimes \mathbf{I}_{N_1})\underline{\mathbf{w}}_{1,r} = (\mathbf{I}_{N_2} \otimes \underline{\mathbf{w}}_{1,r})\underline{\mathbf{w}}_{2,r}$. Accordingly, the weight vector at time k can be

expressed as

$$\underline{\mathbf{w}}(k) = \sum_{r=1}^{\mathcal{R}} \mathbf{A}_{2,r}(k) \underline{\mathbf{w}}_{1,r}(k) = \sum_{r=1}^{\mathcal{R}} \mathbf{A}_{1,r}(k) \underline{\mathbf{w}}_{2,r}(k), \quad (66)$$

where $\mathbf{A}_{2,r}(k) = \underline{\mathbf{w}}_{2,r}(k) \otimes \mathbf{I}_{N_1}$ and $\mathbf{A}_{1,r}(k) = \mathbf{I}_{N_2} \otimes \underline{\mathbf{w}}_{1,r}(k)$, \mathcal{R} is the rank of the ROI NKP RLS-GSC Beamformer. Now, the error can be expressed as

$$e(k) = \underline{\mathbf{g}}_{1R,\mu}^T \underline{\mathbf{u}}(k) - \left(\sum_{r=1}^{\mathcal{R}} \underline{\mathbf{w}}_{2,r}(k) \otimes \underline{\mathbf{w}}_{1,r}(k) \right)^T \underline{\mathbf{u}}_{\text{GSC}}(k). \quad (67)$$

The error of the first filter can be obtained as

$$e_1(k) = \underline{\mathbf{g}}_{1R,\mu}^T \underline{\mathbf{u}}(k) - \sum_{r=1}^{\mathcal{R}} \underline{\mathbf{w}}_{1,r}^T(k) \underline{\mathbf{u}}_{\text{GSC},2,r}(k), \quad (68)$$

where $\underline{\mathbf{u}}_{\text{GSC},2,r}(k) = \mathbf{A}_{2,r}^T(k) \underline{\mathbf{u}}_{\text{GSC}}(k)$ and

$$\underline{\mathbf{u}}_{\text{GSC},2}(k) = [\underline{\mathbf{u}}_{\text{GSC},2,1}^T(k), \dots, \underline{\mathbf{u}}_{\text{GSC},2,\mathcal{R}}^T(k)]^T, \quad (69)$$

$$\underline{\mathbf{w}}_1(k) = [\underline{\mathbf{w}}_{1,1}^T(k), \dots, \underline{\mathbf{w}}_{1,\mathcal{R}}^T(k)]^T. \quad (70)$$

Similarly, the error of the second filter can be obtained as

$$e_2(k) = \underline{\mathbf{g}}_{1R,\mu}^T \underline{\mathbf{u}}(k) - \sum_{r=1}^{\mathcal{R}} \underline{\mathbf{w}}_{2,r}^T(k) \underline{\mathbf{u}}_{\text{GSC},1,r}(k), \quad (71)$$

where $\underline{\mathbf{u}}_{\text{GSC},1,r}(k) = \mathbf{A}_{1,r}^T(k) \underline{\mathbf{u}}_{\text{GSC}}(k)$ and

$$\underline{\mathbf{u}}_{\text{GSC},1}(k) = [\underline{\mathbf{u}}_{\text{GSC},1,1}^T(k), \dots, \underline{\mathbf{u}}_{\text{GSC},1,\mathcal{R}}^T(k)]^T, \quad (72)$$

$$\underline{\mathbf{w}}_2(k) = [\underline{\mathbf{w}}_{2,1}^T(k), \dots, \underline{\mathbf{w}}_{2,\mathcal{R}}^T(k)]^T. \quad (73)$$

The RLS cost functions for $e_1(k)$ and $e_2(k)$ can be expressed as

$$J[\underline{\mathbf{w}}_1(k)] = \sum_{n=1}^k \beta_1^{k-n} e_1^2(n), \quad (74)$$

$$J[\underline{\mathbf{w}}_2(k)] = \sum_{n=1}^k \beta_2^{k-n} e_2^2(n), \quad (75)$$

where $0 < \beta_1 < 1$ and $0 < \beta_2 < 1$ are the forgetting factors of the two smaller filters. The weight update of the first filter can be obtained as

$$\mathbf{h}_{\text{GSC},1}(k) = \mathbf{C}_{\text{GSC},2}^{-1}(k) \underline{\mathbf{u}}_{\text{GSC},2}(k), \quad (76)$$

$$\underline{\mathbf{w}}_1(k) = \underline{\mathbf{w}}_1(k-1) + e_1(k) \mathbf{h}_{\text{GSC},1}(k). \quad (77)$$

The weight update of the second filter can be obtained as

$$\mathbf{h}_{\text{GSC},2}(k) = \mathbf{C}_{\text{GSC},1}^{-1}(k) \underline{\mathbf{u}}_{\text{GSC},1}(k), \quad (78)$$

$$\underline{\mathbf{w}}_2(k) = \underline{\mathbf{w}}_2(k-1) + e_2(k) \mathbf{h}_{\text{GSC},2}(k). \quad (79)$$

The final adaptive weights of the proposed beamformer can be expressed as

$$\underline{\mathbf{w}} = \sum_{r=1}^{\mathcal{R}} \underline{\mathbf{w}}_{2,r} \otimes \underline{\mathbf{w}}_{1,r}. \quad (80)$$

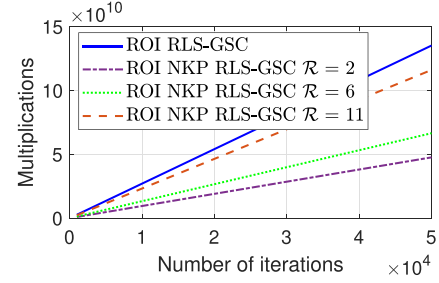


Fig. 5. Number of multiplications with respect to iterations for ROI RLS-GSC and ROI NKP RLS-GSC for ranks $\mathcal{R} \in \{2, 6, 11\}$.

The final weights of the proposed ROI NKP RLS-GSC beamformer can be written as

$$\underline{\mathbf{g}} = \underline{\mathbf{g}}_1 - \mathbf{B}_\Omega \left(\sum_{r=1}^{\mathcal{R}} \underline{\mathbf{w}}_{2,r} \otimes \underline{\mathbf{w}}_{1,r} \right). \quad (81)$$

The computational cost of ROI RLS-GSC and ROI NKP RLS-GSC beamformer can be summarized as follows: ROI RLS-GSC requires $6N^2 + 4N$ multiplications, while ROI NKP RLS-GSC requires $(3\mathcal{R}N_1)^2 + (3\mathcal{R}N_2)^2 + 4\mathcal{R}N_1 + 4\mathcal{R}N_2 + 2N^2 + N(2 + 3\mathcal{R})$ multiplications per iteration. From Fig. 5, it is evident that ROI RLS-GSC requires substantially more multiplications compared to ROI NKP RLS-GSC for $\mathcal{R} \in \{2, 6, 11\}$, with an increase in the number of iterations. Consequently, its total computational cost grows rapidly with the number of iterations. In contrast, ROI NKP RLS-GSC leverages Kronecker product decomposition, resulting in a considerable reduction in the number of multiplications. Thus, the NKP-based approach offers a more computationally efficient alternative.

IV. PERFORMANCE MEASURES

This section defines several metrics for evaluating the performance of the proposed ROI-GSC beamformer. The desired signal received by the reference sensor, $s_1(k)$, is assumed to be white. This assumption enables us to handle broadband desired signals without requiring specific statistical information. The output variance of the beamformer is given by

$$\begin{aligned} \sigma_y^2 &= \underline{\mathbf{g}}^T \mathbf{C}_{\underline{\mathbf{u}}} \underline{\mathbf{g}} \\ &= \sigma_{s_{\text{fd}}}^2 + \sigma_{v_m}^2, \end{aligned} \quad (82)$$

where $\sigma_{s_{\text{fd}}}^2$ and $\sigma_{v_m}^2$ denote the variances of the filtered desired signal and residual noise, respectively:

$$\sigma_{s_{\text{fd}}}^2 = \underline{\mathbf{g}}^T \mathbf{R}(\theta_q, \phi_q) \mathbf{C}_{\bar{s}_1} \mathbf{R}^T(\theta_q, \phi_q) \underline{\mathbf{g}} \quad (83)$$

$$= \underline{\mathbf{g}}^T \mathbf{C}_{\underline{\mathbf{s}}} \underline{\mathbf{g}},$$

$$\sigma_{v_m}^2 = \underline{\mathbf{g}}^T \mathbf{C}_{\underline{\mathbf{v}}} \underline{\mathbf{g}}. \quad (84)$$

Signal leakage represents the portion of the desired signal that is suppressed by the blocking matrix. In the GSC framework, the signal leakage of the desired signal is given by

$$s_l(k) = \underline{\mathbf{g}}_2^T \underline{\mathbf{s}}(k), \quad (85)$$

and its variance is given by

$$\sigma_{s_1}^2 = \underline{\mathbf{g}}_2^T \mathbf{C}_{\bar{\mathbf{s}}_1} \underline{\mathbf{g}}_2. \quad (86)$$

The signal leakage factor of a GSC beamformer for a particular direction (θ, ϕ) is

$$\begin{aligned} \xi_{sl}(\underline{\mathbf{g}}_2, \theta, \phi) &= \frac{\sigma_{s_1}^2}{\sigma_{s_1}^2} \\ &= \frac{\underline{\mathbf{g}}_2^T \mathbf{R}(\theta, \phi) \mathbf{C}_{\bar{\mathbf{s}}_1} \mathbf{R}^T(\theta, \phi) \underline{\mathbf{g}}_2}{\sigma_{s_1}^2} \\ &= \underline{\mathbf{g}}_2^T \mathbf{R}(\theta, \phi) \mathbf{R}^T(\theta, \phi) \underline{\mathbf{g}}_2, \end{aligned} \quad (87)$$

where $\sigma_{s_1}^2$ denotes the variance of the signal $s_1(k)$. Finally, the signal leakage factor for an ROI is defined as

$$\begin{aligned} \xi_{sl,\Omega}(\underline{\mathbf{g}}_2, \theta, \phi) \\ &= \frac{1}{|\Omega|} \iint_{(\theta, \phi) \in \Omega} \underline{\mathbf{g}}_2^T \mathbf{R}(\theta, \phi) \mathbf{R}^T(\theta, \phi) \underline{\mathbf{g}}_2 \sin \theta d\phi d\theta. \end{aligned} \quad (88)$$

The output SNR for a particular direction (θ, ϕ) can be obtained from (83) and (84) and is expressed as

$$\begin{aligned} \text{oSNR}(\underline{\mathbf{g}}, \theta, \phi) &= \frac{\sigma_{s_{fd}}^2}{\sigma_{v_m}^2} \\ &= \frac{\underline{\mathbf{g}}^T \mathbf{R}(\theta, \phi) \mathbf{C}_{\bar{\mathbf{s}}_1} \mathbf{R}^T(\theta, \phi) \underline{\mathbf{g}}}{\underline{\mathbf{g}}^T \mathbf{C}_{\mathbf{v}} \underline{\mathbf{g}}} \\ &= \frac{\sigma_{s_1}^2}{\sigma_{v_1}^2} \times \frac{\underline{\mathbf{g}}^T \mathbf{R}(\theta, \phi) \mathbf{R}^T(\theta, \phi) \underline{\mathbf{g}}}{\underline{\mathbf{g}}^T \mathbf{\Gamma}_{\mathbf{v}} \underline{\mathbf{g}}}. \end{aligned} \quad (89)$$

The input SNR can be obtained from the observation signal received at the reference sensor $\mathbf{u}_1(k) = \mathbf{s}_1(k) + \mathbf{v}_1(k)$, and is expressed as

$$\begin{aligned} \text{iSNR} &= \frac{\text{tr}[\mathbf{C}_{\mathbf{s}_1}]}{\text{tr}[\mathbf{C}_{\mathbf{v}_1}]} \\ &= \frac{\sigma_{s_1}^2}{\sigma_{v_1}^2}, \end{aligned} \quad (90)$$

where $\mathbf{C}_{\mathbf{s}_1}$ and $\mathbf{C}_{\mathbf{v}_1}$ are the covariance matrices of $\mathbf{s}_1(k)$ and $\mathbf{v}_1(k)$, respectively. The array gain for a signal that arrives from the direction (θ, ϕ) is given as

$$\begin{aligned} \mathcal{G}(\underline{\mathbf{g}}, \theta, \phi) &= \frac{\text{oSNR}(\underline{\mathbf{g}}, \theta, \phi)}{\text{iSNR}} \\ &= \frac{\underline{\mathbf{g}}^T \mathbf{R}(\theta, \phi) \mathbf{R}^T(\theta, \phi) \underline{\mathbf{g}}}{\underline{\mathbf{g}}^T \mathbf{\Gamma}_{\mathbf{v}} \underline{\mathbf{g}}}. \end{aligned} \quad (91)$$

The average output SNR for an ROI is

$$\begin{aligned} \text{oSNR}_{\Omega}(\underline{\mathbf{g}}) \\ &= \frac{\sigma_{s_1}^2}{\sigma_{v_1}^2} \times \frac{\frac{1}{|\Omega|} \iint_{(\theta, \phi) \in \Omega} \underline{\mathbf{g}}^T \mathbf{R}(\theta, \phi) \mathbf{R}^T(\theta, \phi) \underline{\mathbf{g}} \sin \theta d\phi d\theta}{\underline{\mathbf{g}}^T \mathbf{\Gamma}_{\mathbf{v}} \underline{\mathbf{g}}} \\ &= \frac{\sigma_{s_1}^2}{\sigma_{v_1}^2} \times \frac{\underline{\mathbf{g}}^T \mathbf{\Gamma}_{\mathbf{R}, \Omega} \underline{\mathbf{g}}}{\underline{\mathbf{g}}^T \mathbf{\Gamma}_{\mathbf{v}} \underline{\mathbf{g}}}, \end{aligned} \quad (92)$$

The average array gain for an ROI is given as

$$\begin{aligned} G_{\Omega}(\underline{\mathbf{g}}) &= \frac{\text{oSNR}_{\Omega}(\underline{\mathbf{g}})}{\text{iSNR}} \\ &= \frac{\underline{\mathbf{g}}^T \mathbf{\Gamma}_{\mathbf{R}, \Omega} \underline{\mathbf{g}}}{\underline{\mathbf{g}}^T \mathbf{\Gamma}_{\mathbf{v}} \underline{\mathbf{g}}}. \end{aligned} \quad (93)$$

The DF represents the array gain when the diffuse noise is taken into consideration and is expressed as follows for a given ROI:

$$D_{\Omega}(\underline{\mathbf{g}}) = \frac{\underline{\mathbf{g}}^T \mathbf{\Gamma}_{\mathbf{R}, \Omega} \underline{\mathbf{g}}}{\underline{\mathbf{g}}^T \mathbf{\Gamma}_0 \underline{\mathbf{g}}}, \quad (94)$$

where $\mathbf{\Gamma}_0$ is expressed as

$$\mathbf{\Gamma}_0 = \frac{1}{4\pi} \int_0^{\pi} \int_0^{2\pi} \mathbf{R}(\theta, \phi) \mathbf{R}^T(\theta, \phi) \sin \theta d\phi d\theta. \quad (95)$$

The WNG represents the array gain when the noise is assumed to be spatio-temporal white. By replacing $\mathbf{\Gamma}_{\mathbf{v}}$ by an identity matrix of dimension $NL_u \times NL_u$, we obtain the WNG for an ROI as follows:

$$W_{\Omega}(\underline{\mathbf{g}}) = \frac{\underline{\mathbf{g}}^T \mathbf{\Gamma}_{\mathbf{R}, \Omega} \underline{\mathbf{g}}}{\underline{\mathbf{g}}^T \underline{\mathbf{g}}}. \quad (96)$$

For a particular direction (θ, ϕ) , the desired signal reduction factor can be expressed as

$$\begin{aligned} \xi_d(\underline{\mathbf{g}}, \theta, \phi) &= \frac{\sigma_{s_1}^2}{\underline{\mathbf{g}}^T \mathbf{R}(\theta, \phi) \mathbf{C}_{\bar{\mathbf{s}}_1} \mathbf{R}^T(\theta, \phi) \underline{\mathbf{g}}} \\ &= \frac{1}{\underline{\mathbf{g}}^T \mathbf{R}(\theta, \phi) \mathbf{R}^T(\theta, \phi) \underline{\mathbf{g}}}. \end{aligned} \quad (97)$$

In an ROI, the average signal reduction factor is given by

$$\xi_{d,\Omega}(\underline{\mathbf{g}}) = \frac{1}{\underline{\mathbf{g}}^T \mathbf{\Gamma}_{\mathbf{R}, \Omega} \underline{\mathbf{g}}}. \quad (98)$$

The beampattern illustrates the response of a beamformer to a signal coming from a specific direction. The broadband beam-pattern of a beamformer can be obtained as follows:

$$|\mathcal{B}(\underline{\mathbf{g}}, \theta, \phi)|^2 = \underline{\mathbf{g}}^T \mathbf{R}(\theta, \phi) \mathbf{R}^T(\theta, \phi) \underline{\mathbf{g}}. \quad (99)$$

V. SIMULATION STUDY

A. Experimental Setup

The experimental setup involves a reverberant room measuring 5 m in width, 4 m in length, and 6 m in height, as shown in Fig. 6. A linear microphone array of 11 omnidirectional microphones is placed along the y -axis. The spacings between elements of the array are [7.5, 15, 7.5, 5, 2.5, 2.5, 5, 7.5, 15, 7.5] cm. The array is centrally located in the room, and the middle microphone is designated as the reference sensor. A loudspeaker, representing the source of interference, is located at the coordinates [2.983, 1.1294, 3] m. The origin of the spherical coordinate system is at the reference sensor, and the DOAs of the signals arrive from an azimuthal direction $\phi \in [-90^\circ, 90^\circ]$ at a polar angle $\theta = 90^\circ$. Reverberant signals are created by adding reverberation to the speakers' speech through convolution of the anechoic signal with the

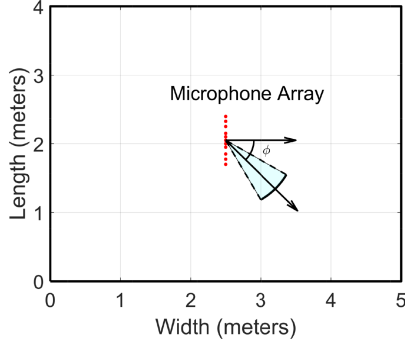


Fig. 6. Schematic of the experimental setup with a microphone array placed in a room measuring 4 meters in length, 5 meters in width, and 6 meters in height. The region-of-interest is represented as a conical sector with azimuthal angle ϕ spanning $[-60^\circ, -30^\circ]$.

room impulse responses from the speakers' locations to the microphones and are generated using the room impulse response generator [56]. For this study, the sampling frequency is $f_s = 16$ kHz, the sound speed is $c = 340$ m/s, and the room reverberation time is set to $RT_{60} = 0.4$ seconds. The source is located $r = 0.68$ m away from the reference microphone and the ROI is $\phi_q \in \Omega = [-60^\circ, -30^\circ]$. The angular range $\Omega = [-60^\circ, -30^\circ]$ was selected as a representative region of interest (ROI) to evaluate the performance of the proposed beamformer. The proposed ROI-GSC framework is not limited to this range and can be extended to different ROIs based on user requirements. The values of L_q and L_u are set to 61 for all simulations. To obtain the matrices required for obtaining the beamformer weights, we simulated a broadband white stationary sound source for $s(k)$ of 1 s duration to propagate from different positions in the room. From (17), we can obtain the cross-correlation matrix using the signals $\underline{s}(k)$ and $\bar{s}_1^T(k + \Delta)$ as follows:

$$\mathbb{E}[\underline{s}(k) \bar{s}_1^T(k + \Delta)] = \underline{\mathbf{R}}(\theta, \phi) \mathbb{E}[\bar{s}_1(k + \Delta) \bar{s}_1^T(k + \Delta)]. \quad (100)$$

Since a broadband white stationary source was used, the covariance of $\bar{s}_1(k + \Delta)$ is approximated by $\sigma_{s_1}^2 \mathbf{I}$, which leads to

$$\underline{\mathbf{R}}(\theta, \phi) = \frac{1}{\sigma_{s_1}^2} \mathbb{E}[\underline{s}(k) \bar{s}_1^T(k + \Delta)]. \quad (101)$$

In practice, the expectation is replaced by a time average over τ samples as follows:

$$\underline{\mathbf{R}}(\theta, \phi) \approx \frac{1}{\sigma_{s_1}^2 \tau} \sum_{k=1}^{\tau} \underline{s}(k) \bar{s}_1^T(k + \Delta). \quad (102)$$

By placing the source at the positions (r, θ, ϕ) , we can obtain the matrices $\underline{\mathbf{R}}_\Omega$ and $\underline{\mathbf{\Gamma}}_{\mathbf{R}, \Omega}$ as follows:

$$\underline{\mathbf{R}}_\Omega = \frac{\sum_k \underline{s}(k, \theta, \phi) \bar{s}_1^T(k + \Delta, \theta, \phi) \sin \theta(k)}{\sigma_{s_1}^2 \sum_k \sin \theta(k)}, \quad (103)$$

$$\underline{\mathbf{\Gamma}}_{\mathbf{R}, \Omega} = \frac{\sum_k \underline{s}(k, \theta, \phi) \underline{s}^T(k, \theta, \phi) \sin \theta(k)}{\sigma_{s_1}^2 \sum_k \sin \theta(k)}. \quad (104)$$

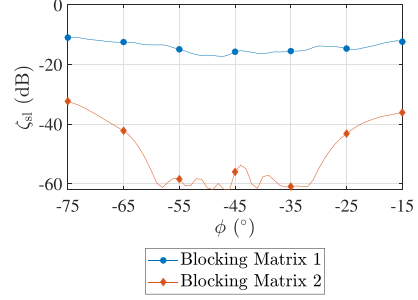


Fig. 7. Signal leakage factor of the proposed ROI-GSC beamformer with Blocking Matrix 1 (46) and Blocking Matrix 2 (47) for the ROI $\Omega = [-60^\circ, -30^\circ]$.

By moving the source along $\phi \in [-90^\circ, 90^\circ]$, we obtained $\underline{\mathbf{\Gamma}}_0$ as follows:

$$\underline{\mathbf{\Gamma}}_0 = \frac{\sum_k \underline{s}(k, \theta, \phi) \underline{s}^T(k, \theta, \phi) \sin \theta(k)}{\sigma_{s_1}^2 \sum_k \sin \theta(k)}. \quad (105)$$

These ROI averaged matrices ($\underline{\mathbf{R}}_\Omega$ and $\underline{\mathbf{\Gamma}}_{\mathbf{R}, \Omega}$) can be obtained by ensuring that the source direction varies slowly and uniformly across the ROI. This can be realized either by rotating the microphone array relative to a fixed source or by rotating the source relative to the array. In this way, the source direction $[\theta(k), \phi(k)]$ becomes uniformly distributed over the ROI Ω , and the recorded signal $s(k)$ becomes a function of $[\theta(k), \phi(k)] \in \Omega$. As a result, the time-averaged sample covariance naturally converges to the ROI averaged matrices, with $\sin \theta(k)$ incorporating the Jacobian factor for a spherical coordinate system. Substantial environmental changes (e.g., relocating to a different room) necessitate a re-estimation of these matrices. To mitigate moderate mismatch without re-estimation, the parameter ϵ_1 can be increased, which improves robustness at the cost of some loss in matched-condition performance. The interferer pseudo-covariance matrix, $\underline{\mathbf{\Gamma}}_{\mathbf{i}}$, was computed using (102) with the source placed at the loudspeaker's location. Finally, the noise pseudo-covariance matrix was taken as a weighted combination of the interferer and spatially white noise: $\underline{\mathbf{\Gamma}}_{\mathbf{v}} = 0.99 \underline{\mathbf{\Gamma}}_{\mathbf{i}} + 0.01 \mathbf{I}_{NL_u}$. This convex mixture captures interference-dominated noise with a smaller white noise component representing sensor noise.

B. Performance Analysis

In this section, the performance of the proposed ROI-GSC beamformer is studied in detail. Fig. 7 compares the signal leakage factor for different choices of the blocking matrix: Blocking Matrix 1 (46) and Blocking Matrix 2 (47) for $\mathcal{L} = 620$ and $\mu = 0.005$. The ROI-GSC beamformer with the proposed Blocking Matrix 2 exhibits superior performance in minimizing signal leakage compared to Blocking Matrix 1. This improvement ensures a more effective blocking of the desired signal while preserving interference and noise components, which is critical for robust beamforming. Due to its enhanced capability, Blocking Matrix 2 has been selected for subsequent simulation studies to ensure more robust performance evaluations. The broadband beampattern of the proposed ROI-GSC beamformer is shown in Fig. 8 for different values of \mathcal{L} , ϵ_0 , ϵ_1 , and μ .

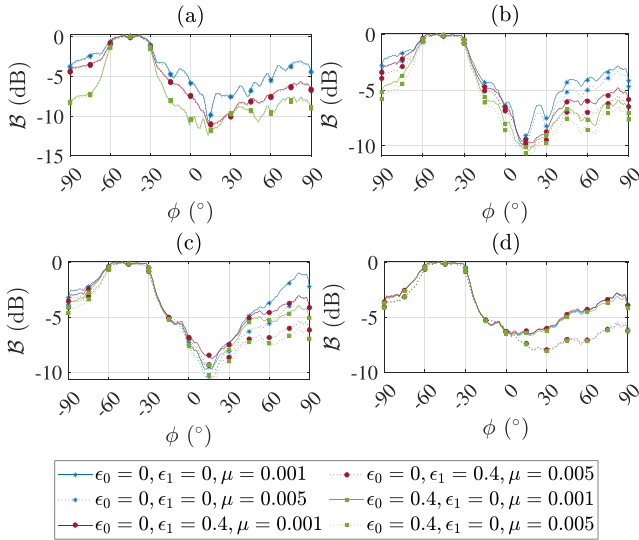


Fig. 8. Broadband beampatterns of the proposed ROI-GSC beamformer for (a) $\mathcal{L} = 240$, (b) $\mathcal{L} = 390$, (c) $\mathcal{L} = 540$, and (d) $\mathcal{L} = 620$, for various values of ϵ_0 , ϵ_1 , and μ .

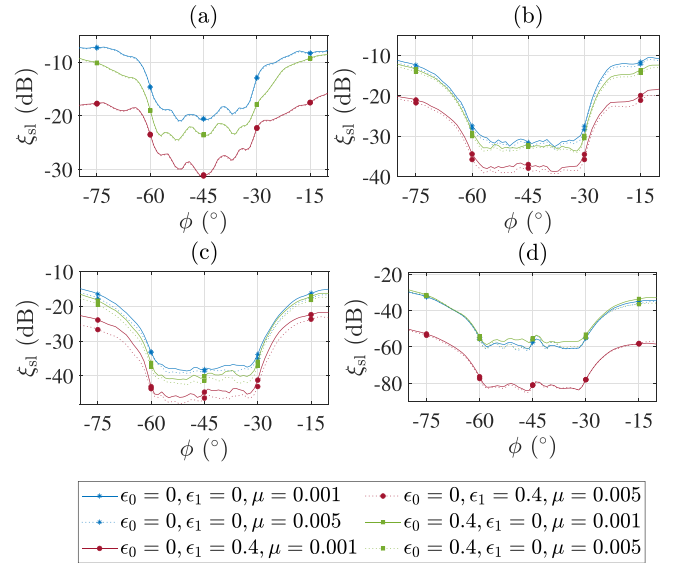


Fig. 10. Signal leakage factor of the proposed ROI-GSC beamformer for (a) $\mathcal{L} = 240$, (b) $\mathcal{L} = 390$, (c) $\mathcal{L} = 540$, and (d) $\mathcal{L} = 620$, for various values of ϵ_0 , ϵ_1 , and μ .

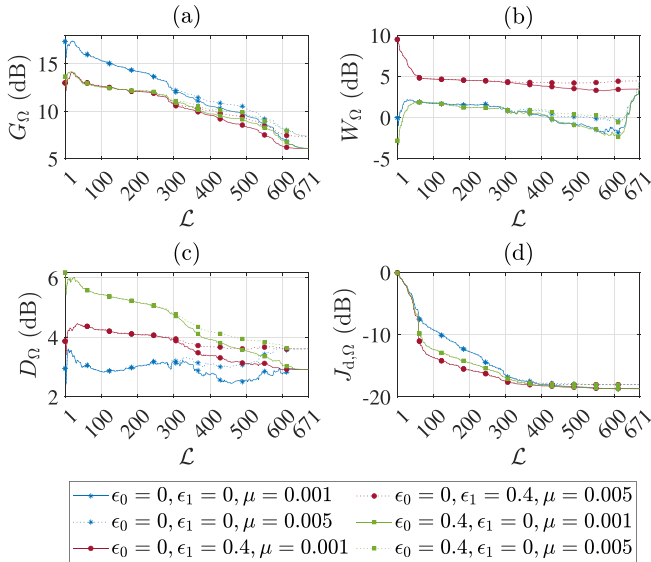


Fig. 9. Performance of proposed ROI-GSC beamformer with respect to \mathcal{L} in terms of average (a) array gain, (b) white noise gain, (c) directivity factor, and (d) distortion, for different values of ϵ_0 , ϵ_1 , and μ .

As \mathcal{L} increases, the beampattern within the ROI approaches 0 dB, indicating reduced distortion. Fig. 9 shows the performance of the proposed ROI-GSC beamformer with respect to \mathcal{L} for different values of ϵ_0 , ϵ_1 , and μ . It can be observed in Fig. 9(a) that the average array gain increases as \mathcal{L} decreases, with $\mathcal{L} = 1$ yielding the highest average gain. However, this higher gain is accompanied by increased distortion, as indicated in Fig. 9(d). Fig. 9(a) shows that for high values of \mathcal{L} , increasing μ further enhances the average array gain. The variation in the average WNG and average DF is depicted in Fig. 9(c) and (d), respectively, showing a performance reduction as \mathcal{L} increases.

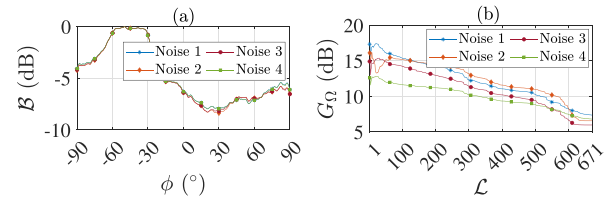


Fig. 11. (a) Beampattern with $\mathcal{L} = 620$ and (b) array gain of the proposed ROI-GSC beamformer for different noises.

Fig. 10 shows plots of the signal leakage factor of the proposed ROI-GSC beamformer for different values of \mathcal{L} , ϵ_0 , ϵ_1 , and μ . The figure indicates that as the value of \mathcal{L} increases, the beamformer's ability to minimize signal leakage within the ROI improves, resulting in more uniform performance over the ROI. Consequently, a tradeoff exists between maximizing array gain and the required level of signal leakage reduction.

Further, we evaluated the proposed ROI-GSC beamformer under four noise conditions with a directional interferer arriving from $[2.983, 1.1294, 3]$ m, represented by $\Gamma_{\mathbf{i}}$. Noise 1: the directional interferer is white noise and is combined with sensor noise, yielding $\Gamma_{\mathbf{v}} = 0.99 \Gamma_{\mathbf{i}} + 0.01 \mathbf{I}_{NL_u}$. Noise 2: the directional interferer is colored and is combined with sensor noise, where the coloring follows an AR(2) model with polynomial $1 - 0.9z^{-1} + 0.7z^{-2}$. Noise 3: The interferer is nonstationary: $\Gamma_{\mathbf{i}}$ is estimated from a time-varying variance process and is combined with sensor noise. Nonstationary noise is synthesized by dividing the signal into five equal-length segments with variances 0.1, 0.5, 1.0, 0.3, and 0.8. Noise 4: The directional interferer is white noise. It is combined with diffuse (reverberant) noise and sensor noise, yielding $\Gamma_{\mathbf{v}} = 0.89 \Gamma_{\mathbf{i}} + 0.1 \Gamma_0 + 0.01 \mathbf{I}_{NL_u}$.

Fig. 11 shows beampatterns and average array gain over the ROI as a function of \mathcal{L} across all four conditions, showing

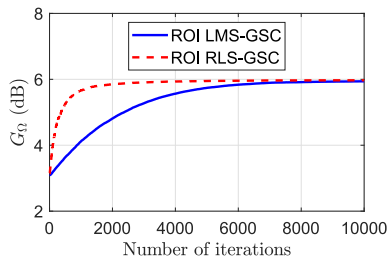


Fig. 12. Array gain vs. the number of iterations of the proposed ROI RLS-GSC beamformer for $\mathcal{L} = \{240, 390, 540, 620\}$ and of (b) the proposed ROI NKP RLS-GSC beamformer for ranks $\mathcal{R} \in \{2, 6, 11\}$ and $\mathcal{L} = 240$.

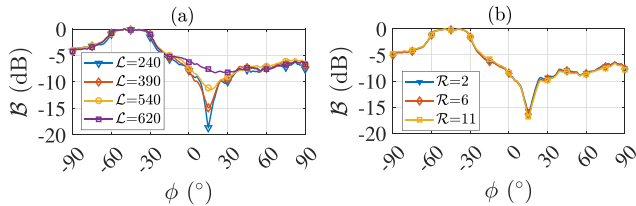


Fig. 13. Broadband beampatterns of (a) the proposed ROI RLS-GSC beamformer for $\mathcal{L} \in \{240, 390, 540, 620\}$ and of (b) the proposed ROI NKP RLS-GSC beamformer for ranks $\mathcal{R} \in \{2, 6, 11\}$ and $\mathcal{L} = 240$.

that the ROI-GSC remains robust under colored, diffuse, and nonstationary interference, with well-defined beampatterns and consistently strong average array gain.

Further, we evaluate the performance of ROI RLS-GSC compared with ROI LMS-GSC in terms of the evolution of the array gain over the iterations. In the ROI RLS-GSC beamformer implementation, the inverse correlation matrix $\mathbf{C}_{\text{GSC}}^{-1}$, associated with the adaptive filter, is initialized as $\mathbf{C}_{\text{GSC}}^{-1}(0) = 0.001 \times \mathbf{I}$, where \mathbf{I} denotes an identity matrix sized to match the length of the adaptive weight vector \mathbf{w}_{gsc} . This initialization helps maintain numerical stability and provides a well-conditioned starting point for the RLS algorithm's first iterations. From Fig. 12, it can be observed that the RLS variant converges significantly faster than the LMS. Specifically, an array gain of 5.9 dB is achieved in approximately 2920 iterations for ROI RLS-GSC, whereas ROI LMS-GSC requires about 7176 iterations to reach the same performance. This highlights the well-known trade-off between the two algorithms: while LMS offers lower computational complexity per iteration, its convergence speed is slower. In contrast, RLS incurs a higher computational cost but provides much faster convergence, making it preferable in scenarios where rapid adaptation is crucial. Fig. 13 shows the broadband beampattern of the proposed ROI RLS-GSC beamformer for different values of \mathcal{L} and of the proposed ROI NKP RLS-GSC beamformer for different values of \mathcal{R} . For every \mathcal{L} , the beampattern is shown after convergence. As \mathcal{R} decreases, the computational complexity decreases, yet the degradation in performance remains minimal. For example, with $\mathcal{R} = 11$, the interference null depth reaches -16.8 dB; reducing the rank to $\mathcal{R} = 6$ results in only a 0.5 dB loss; and further reducing to $\mathcal{R} = 2$ incurs a total degradation of only 1 dB to -15.8 dB. These results demonstrate that substantial computational savings can be achieved by reducing the rank,

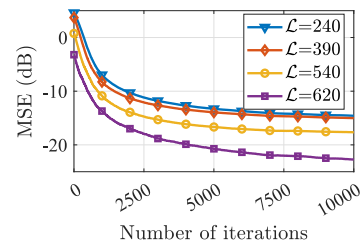


Fig. 14. MSE vs. the number of iterations of the proposed ROI RLS-GSC beamformer for $\mathcal{L} \in \{240, 390, 540, 620\}$.

with only a marginal impact on interference suppression. The adaptive weight vector in the ROI RLS-GSC beamformer, \mathbf{w} , has a length of 671. In contrast, the ROI NKP RLS-GSC beamformer employs two significantly shorter adaptive weight vectors, \mathbf{w}_1 and \mathbf{w}_2 , with lengths $N_1 = 61$ and $N_2 = 11$, respectively. The adaptive weight vectors \mathbf{w}_1 and \mathbf{w}_2 , which correspond to the Kronecker decomposition components, are initialized randomly with zero mean and a variance of 0.001.

Fig. 14 shows the MSE of the proposed ROI RLS-GSC beamformer for different values of \mathcal{L} . As observed, the algorithm successfully converges for all tested values of \mathcal{L} . The adaptive implementation was evaluated under interference with power 0.5625 and noise with power 0.4375. The ROI RLS-GSC requires 2,704,130 multiplications per iteration, whereas the proposed ROI NKP RLS-GSC significantly reduces the complexity to 952,530 multiplications at rank 2 ($\approx 65\%$ reduction) and 1,330,566 multiplications at rank 6 ($\approx 51\%$ reduction). Despite this reduction, the average array gain over the ROI has only a slight reduction, with 8.4 dB for ROI RLS-GSC, compared to 8.3 dB ($\mathcal{R} = 2$) and 8.4 dB ($\mathcal{R} = 6$) for ROI NKP RLS-GSC. These results confirm that even though low-rank approximation is applied, the performance degradation is minimal, with only a slight loss relative to ROI RLS-GSC. Thus, the proposed ROI NKP RLS-GSC framework offers a tradeoff between complexity and performance, providing a practical, low-complexity variant of the ROI RLS-GSC beamformer that remains robust while enabling a low-complexity implementation.

C. Comparative Analysis of Baseline Algorithms

In this section, we benchmark the ROI-GSC beamformer against three baseline algorithms: the robust GSC (R-GSC) [12], the Normal MVDR (N-MVDR) [31], and robust LCMV (R-LCMV) [57]. For the ROI-GSC setup, we select $\mathcal{L} = 620$, $\mu = 0$, and $\Omega = [-60^\circ, -30^\circ]$, while the R-GSC assumes $\phi_q = -45^\circ$. A regularization factor of 0.0547 is applied to match the average array gain of ROI-GSC and R-GSC, and is used consistently across all baselines with $\epsilon_0 = 0$ and $\epsilon_1 = 0.1$. The N-MVDR enforces a unit average distortion over the ROI employing a normal spatial distribution with a standard deviation of 4.5° , centered at $(-45^\circ, 0^\circ)$. At the same time, the robust LCMV applies multiple distortionless constraints at all azimuth positions within the ROI. Although the proposed N-MVDR was originally implemented in the frequency domain, we reformulated it in the time domain. In Fig. 15, the performances of the

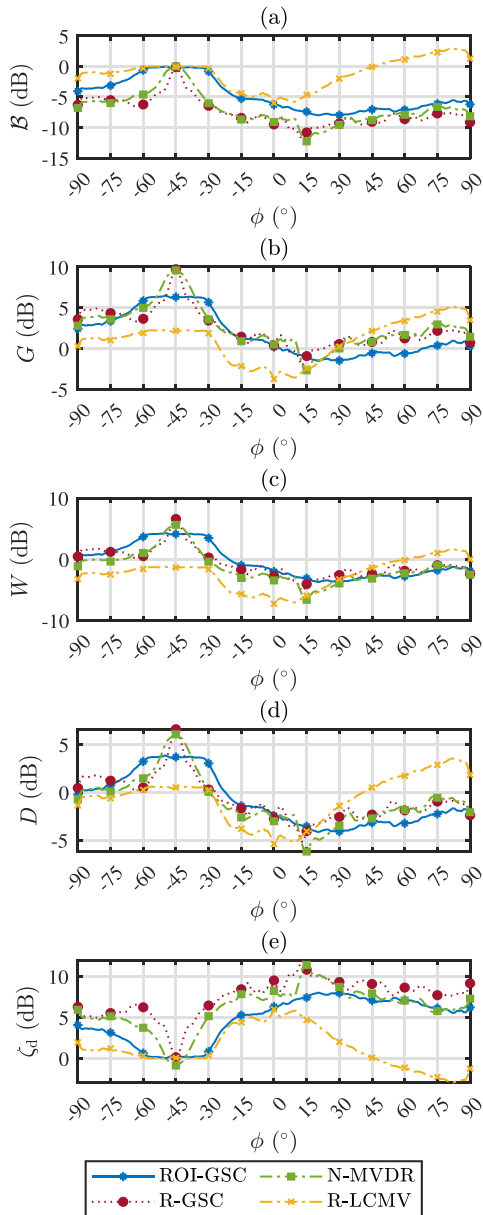


Fig. 15. Beampattern and performance metrics of ROI-GSC, R-GSC, N-MVDR, R-LCMV beamformers analyzed as functions of the DOA in terms of (a) broadband beampattern, (b) array gain, (c) white noise gain, (d) directivity factor, and (e) distortion.

proposed ROI-GSC beamformer compared to the R-GSC, N-MVDR, and R-LCMV beamformers are analyzed as functions of the DOA in terms of beampattern, array gain, WNG, DF, and desired signal reduction factor. The R-GSC and N-MVDR beamformers are designed for $\phi_q = -45^\circ$. At $\phi = -45^\circ$, the R-GSC and N-MVDR provide better array gain and lower distortion. The N-MVDR achieves higher array gain over a broader angular region compared to the R-GSC. However, as the angle deviates from $\phi = -45^\circ$, the proposed ROI beamformer surpasses the R-GSC and N-MVDR, achieving a higher array

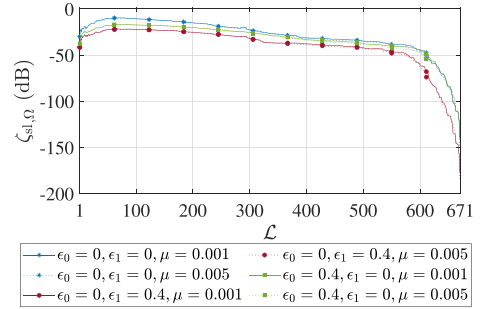


Fig. 16. Signal leakage factor of the proposed ROI-GSC beamformer with respect to \mathcal{L} for different values of ϵ_0 , ϵ_1 , and μ .

gain and reduced distortion, as can be observed from Figs. 15(b) and (e). The same trend can be observed for WNG in Fig. 15(c) and DF in Fig. 15(d): while the R-GSC and N-MVDR perform better at $\phi = -45^\circ$, their performance degrades outside this angle. However, as the angle deviates further from the nominal direction, the proposed ROI-GSC beamformer provides more consistent array gain across the ROI while incurring less signal distortion. In contrast, although the R-LCMV enforces unity gain within the ROI and achieves low signal distortion in that region, it suffers from poor array gain, reduced WNG, and lower DF.

For the ROI-GSC beamformer, the primary computational burden arises from two operations. One is obtaining the noise correlation matrix $\mathbf{\Gamma}_{\mathbf{v}, \epsilon}$ and the other is diagonalizing the ROI correlation matrix $\mathbf{\Gamma}_{\mathbf{R}, \Omega}$. In particular, evaluating the product $\mathbf{R}(\theta, \phi)\mathbf{R}^T(\theta, \phi)$ requires $L(NL_u)^2$ multiplications for each angular direction. When the angular integral is discretized over $|\Omega_q|$ grid points, the total complexity of computing $\mathbf{\Gamma}_0$ for all directions scales as $\mathcal{O}(|\Omega_d| L(NL_u)^2)$. Further, diagonalization of the resulting $NL_u \times NL_u$ matrix contributes an additional $\mathcal{O}((NL_u)^3)$ operations. The R-GSC and N-MVDR beamformers entail a comparable computational cost with respect to the ROI-GSC beamformer since it also requires evaluating $\mathbf{\Gamma}_{\mathbf{v}, \epsilon}$. Furthermore, the optimization stage involves matrix multiplications and inversions of comparable size, resulting in an overall computational cost of $\mathcal{O}((NL_u)^3)$. In the case of the R-LCMV beamformer, it specifically requires inverting a $31L \times 31L$ matrix, incurring a higher computational cost. Finally, applying the spatiotemporal filter coefficients of the respective beamformer to the sensor observations entails an additional NL_u multiplications for all of the beamformers.

In Fig. 16, the average signal leakage factor of the proposed ROI-GSC beamformer with respect to \mathcal{L} for different values of ϵ_0 , ϵ_1 , and μ is shown. It can be observed from the figure that the average signal leakage factor of the array decreases as the value of \mathcal{L} increases, resulting in reduced distortion of the desired signal. Fig. 17 illustrates the signal leakage factor of the proposed ROI-GSC beamformer with that of Zheng et al. [38] and the conventional GSC beamformer. The settings of the ROI-GSC beamformer are for an ROI $\Omega = [-60^\circ, -30^\circ]$, $\mathcal{L} = 620$, $\epsilon_0 = \epsilon_1 = 0$, and $\mu = 0.005$. The beamformer proposed by Zheng et al. [38] is used for comparison and is designed

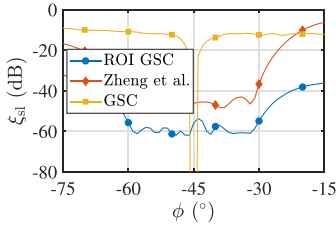


Fig. 17. Comparison of the ROI-GSC beamformer, the GSC beamformer, and the method of Zheng et al. [38] in terms of signal leakage factor in the ROI $\phi \in \Omega$.

for an ROI $\Omega = [-60^\circ, -30^\circ]$ with an azimuthal resolution of 1° . It operates in the frequency range $[2, 8000]$ Hz, using 1000 frequency points within this band. Additionally, the singular value decomposition of the constraint matrix is performed, and the matrix is reconstructed using a low-rank approximation with a rank of 280. As shown in the figure, the GSC beamformer effectively blocks signals only at $\phi = -45^\circ$, outperforming the proposed beamformer in that specific direction. However, its signal leakage increases as the angle deviates from $\phi = -45^\circ$ within the ROI. The figure demonstrates that the proposed ROI-GSC beamformer achieves a lower signal leakage factor compared with the method by Zheng et al. [38]. This performance comparison was conducted under the condition of the same average array gain for all the beamformers. The results demonstrate that the proposed ROI-GSC beamformer offers consistent performance across the ROI, leading to improved robustness and reduced leakage.

D. Speech Simulations

In this section, we evaluate the speech leakage of the proposed ROI RLS-GSC beamformer. Although the proposed ROI RLS-GSC beamformer allows continuous filter adaptation, a slight distortion of the desired speech can still occur due to signal leakage. This leakage arises when the blocking matrix does not perfectly eliminate the target speech from the sidelobe canceller path, allowing a portion of the desired signal to enter the adaptive noise cancellation branch. Consequently, the adaptive filter may inadvertently cancel the leaked desired signal along with the interference, leading to distortion of the desired speech. Our simulation results support this observation as shown in Fig. 18: at $\mathcal{L} = 240$, the amount of leaked target signal (and the resulting speech distortion) was appreciably higher, whereas at $\mathcal{L} = 620$ the leakage and distortion were considerably reduced yet not eliminated. Furthermore, increasing the number of eigenvectors improved leakage suppression, albeit at the expense of array gain, underscoring the inherent tradeoff between preserving the desired signal and suppressing interference. It should also be noted that in this work, we have not included any update control mechanisms in the adaptive stage; however, such strategies can be incorporated in the proposed algorithm to enhance robustness against desired signal cancellation further. Furthermore, we evaluate the performance of the proposed ROI-GSC beamformer in comparison to the method of Zheng et al. [38] using speech signals. The interference signal used is a speech signal, while the

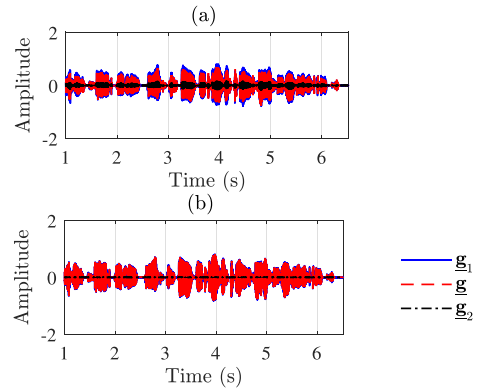


Fig. 18. Beamformer outputs of the proposed ROI RLS-GSC: the data-independent branch output (corresponding to weights \underline{g}_1), the data-dependent adaptive branch output (corresponding to weights \underline{g}_2), and the final combined beamformer output (with weights \underline{g}) for (a) $\mathcal{L} = 240$ and (b) $\mathcal{L} = 620$.

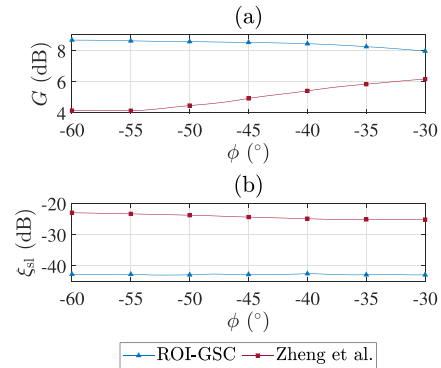


Fig. 19. The performance metrics of the proposed ROI-GSC beamformer and Zheng et al. [38] analyzed as functions of the DOA, and the average performances over the ROI using speech signals in terms of (a) array gain and (b) signal leakage factor. The settings of the ROI-GSC beamformer: $\Omega = [-60^\circ, -30^\circ]$, $\mathcal{L} = 620$, $\epsilon_0 = \epsilon_1 = 0$, $\mu = 0.005$ and the GSC beamformer is designed for $\phi_q = -45^\circ$.

white noise is set to 0.01 times the noise variance in the reference sensor, with the input SNR set at -10 dB. To perform speech simulations, both the proposed ROI-GSC and Zheng et al. [38] beamformers are applied to the same input signals. The speech signals, along with the interference and noise components, are processed through these weights to evaluate the performance of each filter. The following performance metrics are used for evaluation:

$$\text{iSNR} = \frac{\text{var}[s_1(k)]}{\text{var}[v_1(k)]}, \quad (106)$$

$$\text{oSNR}(\underline{g}, \theta_q, \phi_q) = \frac{\text{var}[s_{fd}(k)]}{\text{var}[v_m(k)]}, \quad (107)$$

$$G(\underline{g}, \theta_q, \phi_q) = \frac{\text{oSNR}(\underline{g}, \theta_q, \phi_q)}{\text{iSNR}}, \quad (108)$$

$$\xi_{sl}(\underline{g}, \theta_q, \phi_q) = \frac{\text{var}[s_l(k)]}{\text{var}[s_1(k)]}, \quad (109)$$

where $\text{var}(\cdot)$ represents the empirical variance of the signals. The desired signal comprises English speech from a female speaker,

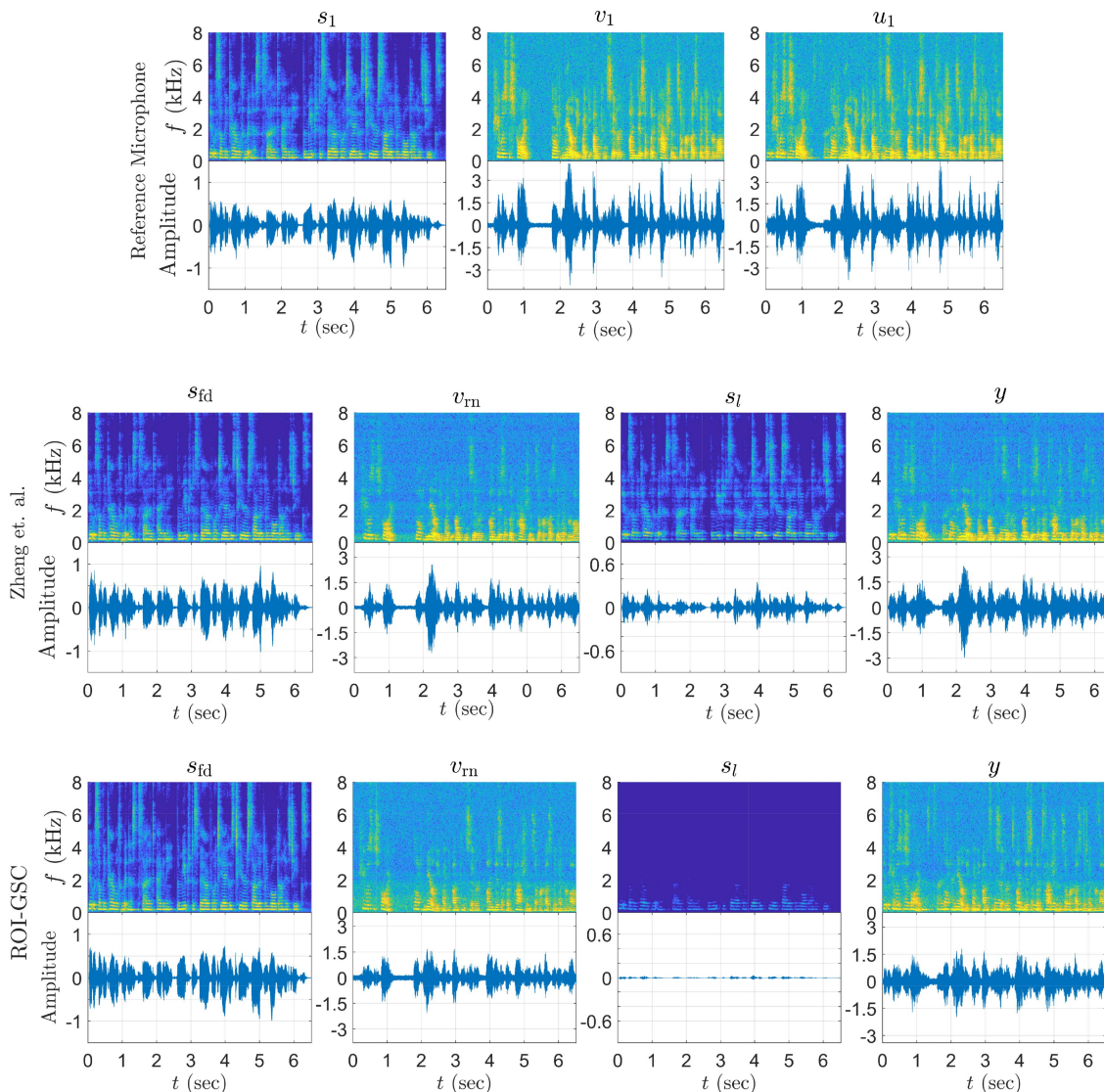


Fig. 20. Spectrograms and waveforms of the input speech s_1 , input noise v_1 , input signal at the reference microphone u_1 , filtered desired signal s_{fd} , residual noise v_{rn} , leakage signal s_l , and beamformer output y for both the methods of Zheng et al. [38] and the proposed ROI-GSC. The desired source direction is at $\phi_q = -33^\circ$ with an input SNR of -10 dB. The settings of the ROI-GSC beamformer: $\Omega = [-60^\circ, -30^\circ]$, $\mathcal{L} = 620$, $\epsilon_0 = 0$, $\epsilon_1 = 0.01$, and $\mu = 0.005$.

whereas the interference signal is from a male speaker. The desired signal direction was set at $\phi_q = -33^\circ$. Fig. 19 presents the performance metrics of the proposed ROI-GSC and Zheng et al. [38] beamformers as functions of the DOA, and the average performances over the ROI, evaluated using 20 speech samples from the LibriSpeech dataset [58]. The proposed beamformer achieves higher array gain and lower signal leakage compared to Zheng et al. [38]. The difference in array gain in Fig. 19(a) relative to Fig. 15(a) is attributed to the mismatch between the white noise assumption used in the theoretical model and the actual speech signal distribution. The beamformer of Zheng et al. [38] yields an average signal leakage factor of -24 dB, while the proposed ROI-GSC achieves -43 dB, demonstrating the effectiveness of our proposed design. Fig. 20 displays the spectrograms and waveforms of the input speech, noise, and reference microphone signal, as well as the filtered outputs and

leakage signals for both beamformers. The desired signal and noise signal, when passed through the Zheng et al. [38] beamformer and the ROI-GSC beamformer, are shown along with the signal leakage plots. The proposed beamformer exhibits visibly lower signal leakage than the state-of-the-art beamformer, which contributes to improved signal quality.

VI. CONCLUSION

We have introduced a novel time-domain optimal beamformer that integrates the ROI framework into the GSC structure. This design enhances signals arriving from a specified ROI while suppressing noise and interference from other directions, making it particularly suitable when precise source location information is unavailable. Additionally, an adaptive implementation based on the LMS and RLS algorithms was developed, along with a

low-complexity variant of RLS using the NKP method. Simulation results confirmed the beamformer's ability to maintain low distortion for sources within the ROI while effectively suppressing noise and interference. We also demonstrated that varying the number of eigenvectors provides a tunable tradeoff between array gain and signal distortion. To minimize signal leakage, we derived a blocking matrix tailored to suppress desired signal components that originate from within the ROI. In addition, dedicated performance metrics were introduced to quantify signal leakage, enabling a systematic evaluation of how the number of eigenvectors used in the blocking matrix affects signal leakage and array gain. Increasing the number of eigenvectors improved leakage suppression at the expense of array gain, highlighting the tradeoff between the two. Finally, we compared the proposed ROI-GSC beamformer with the conventional GSC and a state-of-the-art beamformer. The results show that the proposed method outperforms the conventional GSC in scenarios with uncertain source direction, whereas the conventional GSC remains advantageous when the desired direction of the source is accurately known.

REFERENCES

- [1] J. Benesty, I. Cohen, and J. Chen, *Fundamentals of Signal Enhancement and Array Signal Processing*. Hoboken, NJ, USA: Wiley, 2018.
- [2] H. L. Van Trees, *Optimum Array Processing: Part IV of Detection, Estimation, and Modulation Theory*. New York, NY, USA: Wiley, 2002.
- [3] P. Chiariotti, M. Martarelli, and P. Castellini, "Acoustic beamforming for noise source localization—reviews, methodology and applications," *Mech. Syst. Signal Process.*, vol. 120, pp. 422–448, 2019.
- [4] B. J. Cho, J.-M. Lee, and H.-M. Park, "A beamforming algorithm based on maximum likelihood of a complex gaussian distribution with time-varying variances for robust speech recognition," *IEEE Signal Process. Lett.*, vol. 26, no. 9, pp. 1398–1402, Sep. 2019.
- [5] W. Zhang et al., "End-to-end dereverberation, beamforming, and speech recognition with improved numerical stability and advanced frontend," in *Proc. IEEE Int. Conf. Acoust., Speech Signal Process.*, 2021, pp. 6898–6902.
- [6] J. Benesty, J. Chen, Y. Huang, and I. Cohen, *Noise Reduction in Speech Processing*, vol. 14. Berlin, Germany: Springer, 2009.
- [7] G. Itzhak, J. Benesty, and I. Cohen, "On the design of differential kronecker product beamformers," *IEEE/ACM Trans. Audio, Speech, Lang. Process.*, vol. 29, pp. 1397–1410, 2021.
- [8] D. H. Johnson and D. E. Dudgeon, *Array Signal Processing: Concepts and Techniques*. Englewood Cliffs, NJ, USA: Simon and Schuster, 1992.
- [9] B. D. Van Veen and K. M. Buckley, "Beamforming: A versatile approach to spatial filtering," *IEEE ASSP Mag.*, vol. 5, no. 2, pp. 4–24, Apr. 1988.
- [10] J. M. Kates, "Speech processing in modern communication: Challenges and perspectives," *J. Acoustical Soc. America*, vol. 129, no. 1, pp. 535–535, 2011.
- [11] L. C. De Silva, C. Morikawa, and I. M. Petra, "State of the art of smart homes," *Eng. Appl. Artif. Intell.*, vol. 25, no. 7, pp. 1313–1321, 2012.
- [12] K. Buckley and L. Griffiths, "An adaptive generalized sidelobe canceller with derivative constraints," *IEEE Trans. Antennas Propag.*, vol. 34, no. 3, pp. 311–319, Mar. 1986.
- [13] N. Jablon, "Adaptive beamforming with the generalized sidelobe canceller in the presence of array imperfections," *IEEE Trans. Antennas Propag.*, vol. 34, no. 8, pp. 996–1012, Aug. 1986.
- [14] K. Buckley, "Broad-band beamforming and the generalized sidelobe canceller," *IEEE Trans. Acoust., Speech, Signal Process.*, vol. 34, no. 5, pp. 1322–1323, Oct. 1986.
- [15] I. Cohen, "Analysis of two-channel generalized sidelobe canceller (GSC) with post-filtering," *IEEE Speech Audio Process.*, vol. 11, no. 6, pp. 684–699, Nov. 2003.
- [16] G. Reuven, S. Gannot, and I. Cohen, "Dual-source transfer-function generalized sidelobe canceller," *IEEE Trans. Audio, Speech, Lang. Process.*, vol. 16, no. 4, pp. 711–727, May 2008.
- [17] J. Bitzer, K. U. Simmer, and K.-D. Kammeyer, "Theoretical noise reduction limits of the generalized sidelobe canceller (GSC) for speech enhancement," in *Proc. IEEE Int. Conf. Acoust., Speech, Signal Process.*, 1999, vol. 5, pp. 2965–2968.
- [18] J. H. Doles and F. Benedict, "Broad-band array design using the asymptotic theory of unequally spaced arrays," *IEEE Trans. Antennas Propag.*, vol. 36, no. 1, pp. 27–33, Jan. 1988.
- [19] T. Chou, "Frequency-independent beamformer with low response error," in *Proc. IEEE Int. Conf. Acoust., Speech, Signal Process.*, 1995, vol. 5, pp. 2995–2998.
- [20] J. Marciano, Jr and T. Vu, "Reduced complexity beam space broadband frequency invariant beamforming," *Electron. Lett.*, vol. 36, no. 7, 2000, Art. no. 1.
- [21] E. Mabande and W. Kellermann, "Design of robust polynomial beamformers as a convex optimization problem," in *Proc. IEEE Int. Workshop Acoust. Echo, Noise Control*, 2010, pp. 1–4.
- [22] W. Zhu and W. Wu, "Design of wide-band array with frequency invariant beam pattern by using adaptive synthesis method," in *Proc. IEEE Int. Conf. Image Anal. Signal Process.*, 2011, pp. 688–693.
- [23] J. Wang, Q. Feng, R. Wu, and Z. Su, "A constant-beamwidth beamforming method for acoustic imaging," in *Proc. IEEE Antennas Propag. Soc. Int. Symp.*, 2007, pp. 4236–4239.
- [24] O. Rosen, I. Cohen, and D. Malah, "FIR-based symmetrical acoustic beamformer with a constant beamwidth," *Signal Process.*, vol. 130, pp. 365–376, 2017.
- [25] M. M. Goodwin and G. W. Elko, "Constant beamwidth beamforming," in *Proc. IEEE Int. Conf. Acoust., Speech, Signal Process.*, 1993, vol. 1, pp. 169–172.
- [26] T. Long, I. Cohen, B. Berdugo, Y. Yang, and J. Chen, "Window-based constant beamwidth beamformer," *Sensors*, vol. 19, no. 9, 2019, Art. no. 2091.
- [27] R. Sharma, I. Cohen, and B. Berdugo, "Window beamformer for sparse concentric circular array," in *Proc. IEEE Int. Conf. Acoust., Speech Signal Process.*, 2021, pp. 4500–4504.
- [28] R. Sharma, I. Cohen, and B. Berdugo, "Controlling elevation and azimuth beamwidths with concentric circular microphone arrays," *IEEE/ACM Trans. Audio, Speech, Lang. Process.*, vol. 29, pp. 1491–1502, 2021.
- [29] X. Wang, I. Cohen, J. Chen, and J. Benesty, "On robust and high directive beamforming with small-spacing microphone arrays for scattered sources," *IEEE/ACM Trans. Audio, Speech, Lang. Process.*, vol. 27, no. 4, pp. 842–852, Apr. 2019.
- [30] X. Wenmeng, B. Changchun, J. Maoshen, and J. Picheral, "Speech enhancement with robust beamforming for spatially overlapped and distributed sources," *IEEE/ACM Trans. Audio, Speech, Lang. Process.*, vol. 30, pp. 2778–2790, 2022.
- [31] G. Itzhak and I. Cohen, "Robust beamforming for multispeaker audio conferencing under DOA uncertainty," *IEEE/ACM Trans. Audio, Speech, Lang. Process.*, vol. 33, pp. 139–151, 2025.
- [32] A. Davis, S. Y. Low, S. Nordholm, and N. Grbic, "A subband space constrained beamformer incorporating voice activity detection [speech enhancement applications]," in *Proc. IEEE Int. Conf. Acoust., Speech Signal Process.*, 2005, vol. 3, pp. iii/65–iii/68.
- [33] M. Taseska and E. A. Habets, "Spotforming: Spatial filtering with distributed arrays for position-selective sound acquisition," *IEEE/ACM Trans. Audio, Speech, Lang. Process.*, vol. 24, no. 7, pp. 1291–1304, Jul. 2016.
- [34] A. Barnov, V. B. Bracha, S. Markovich-Golan, and S. Gannot, "Spatially robust GSC beamforming with controlled white noise gain," in *Proc. IEEE 16th Int. Workshop Acoust. Signal Enhancement*, 2018, pp. 231–235.
- [35] K. Takao, M. Fujita, and T. Nishi, "An adaptive antenna array under directional constraint," *IEEE Trans. Antennas Propag.*, vol. 24, no. 5, pp. 662–669, Sep. 1976.
- [36] Y. Grenier, "A microphone array for car environments," *Speech Commun.*, vol. 12, no. 1, pp. 25–39, 1993.
- [37] O. Hoshuyama, A. Sugiyama, and A. Hirano, "A robust adaptive beamformer for microphone arrays with a blocking matrix using constrained adaptive filters," *IEEE Trans. Signal Process.*, vol. 47, no. 10, pp. 2677–2684, Oct. 1999.
- [38] Y. R. Zheng, R. A. Goubran, and M. El-Tanany, "Robust near-field adaptive beamforming with distance discrimination," *IEEE Trans. Speech Audio Process.*, vol. 12, no. 5, pp. 478–488, Sep. 2004.
- [39] A. Frank and I. Cohen, "Least-distortion maximum gain beamformer for time-domain region-of-interest beamforming," *IEEE Trans. Audio, Speech Lang. Process.*, vol. 33, pp. 2286–2301, 2025.
- [40] S. Zhang and I. L.-J. Thng, "Robust presteering derivative constraints for broadband antenna arrays," *IEEE Trans. Signal Process.*, vol. 50, no. 1, pp. 1–10, Jan. 2002.

- [41] R. G. Lorenz and S. P. Boyd, "Robust minimum variance beamforming," *IEEE Trans. Signal Process.*, vol. 53, no. 5, pp. 1684–1696, May 2005.
- [42] N. Vervliet, O. Debals, L. Sorber, and L. De Lathauwer, "Breaking the curse of dimensionality using decompositions of incomplete tensors: Tensor-based scientific computing in Big Data analysis," *IEEE Signal Process. Mag.*, vol. 31, no. 5, pp. 71–79, Sep. 2014.
- [43] A. Cichocki et al., "Tensor decompositions for signal processing applications: From two-way to multiway component analysis," *IEEE Signal Process. Mag.*, vol. 32, no. 2, pp. 145–163, Mar. 2015.
- [44] M. Bousse, O. Debals, and L. De Lathauwer, "A tensor-based method for large-scale blind source separation using segmentation," *IEEE Trans. Signal Process.*, vol. 65, no. 2, pp. 346–358, Jan. 2017.
- [45] N. D. Sidiropoulos, L. De Lathauwer, X. Fu, K. Huang, E. E. Papalexakis, and C. Faloutsos, "Tensor decomposition for signal processing and machine learning," *IEEE Trans. Signal Process.*, vol. 65, no. 13, pp. 3551–3582, Jul. 2017.
- [46] C. Paleologu, J. Benesty, and S. Ciochină, "Linear system identification based on a kronecker product decomposition," *IEEE/ACM Trans. Audio, Speech, Lang. Process.*, vol. 26, no. 10, pp. 1793–1808, Oct. 2018.
- [47] I. Cohen, J. Benesty, and J. Chen, "Differential Kronecker product beamforming," *IEEE/ACM Trans. Audio, Speech, Lang. Process.*, vol. 27, no. 5, pp. 892–902, May 2019.
- [48] J. Benesty, I. Cohen, and J. Chen, *Array Processing - Kronecker Product Beamforming. Switzerland: Springer Topics in Signal Processing*, Berlin, Germany: Springer, 2019.
- [49] X. Wang, G. Huang, J. Benesty, J. Chen, and I. Cohen, "Time difference of arrival estimation based on a Kronecker product decomposition," *IEEE Signal Process. Lett.*, vol. 28, pp. 51–55, 2021.
- [50] S. S. Bhattacharjee and N. V. George, "Nearest Kronecker product decomposition based linear-in-the-parameters nonlinear filters," *IEEE/ACM Trans. Audio, Speech, Lang. Process.*, vol. 29, pp. 2111–2122, 2021.
- [51] G. Huang, J. Benesty, I. Cohen, and J. Chen, "Kronecker product multichannel linear filtering for adaptive weighted prediction error-based speech dereverberation," *IEEE/ACM Trans. Audio, Speech, Lang. Process.*, vol. 30, pp. 1277–1289, 2022.
- [52] X. Wang, G. Huang, I. Cohen, J. Benesty, and J. Chen, "Kronecker product adaptive beamforming for microphone arrays," in *Proc. Asia-Pacific Signal Inf. Process. Assoc. Annu. Summit Conf.*, 2021, pp. 49–54.
- [53] X. Wang, J. Benesty, J. Chen, G. Huang, and I. Cohen, "Beamforming with cube microphone arrays via Kronecker product decompositions," *IEEE/ACM Trans. Audio, Speech, Lang. Process.*, vol. 29, pp. 1774–1784, 2021.
- [54] H. Cox, R. Zeskind, and T. Kooij, "Practical supergain," *IEEE Trans. Acoust., Speech, Signal Process.*, vol. 34, no. 3, pp. 393–398, Jun. 1986.
- [55] H. Cox, R. Zeskind, and M. Owen, "Robust adaptive beamforming," *IEEE Trans. Acoust., Speech, Signal Process.*, vol. 35, no. 10, pp. 1365–1376, Oct. 1987.
- [56] E. A. P. Habets, "Room impulse response generator," Technische Universiteit Eindhoven, Tech. Rep, vol. 2, no. 2.4, 2006, Art. no. 1.
- [57] O. L. Frost, "An algorithm for linearly constrained adaptive array processing," in *Proc. IEEE*, vol. PROC-60, no. 8, Aug. 1972, pp. 926–935.
- [58] V. Panayotov, G. Chen, D. Povey, and S. Khudanpur, "Librispeech: An ASR corpus based on public domain audio books," in *Proc. IEEE Int. Conf. Acoust., Speech Signal Process.*, 2015, pp. 5206–5210.